Journal of Waterway, Port, Coastal, and Ocean Engineering. Submitted November 29, 2012; accepted May 2, 2013; posted ahead of print May 4, 2013. doi:10.1061/(ASCE)WW.1943-5460.0000210

A comprehensive field study of swash-zone processes, Part 1: Experimental design with examples of hydrodynamic and sediment transport measurements

Jack A. Puleo[*1], Chris Blenkinsopp[2], Daniel Conley[3], Gerd Masselink[4], Ian L. Turner[5] , Paul Russell[6], Daniel Buscombe[7], Daniel Howe[8], Thijs Lanckriet[9], Robert McCall[10] and Timothy Poate[11]

[*]Corresponding author

1 Associate Professor, Center for Applied Coastal Research, Ocean Engineering Bldg., University of Delaware, Newark, DE 19716, jpuleo@udel.edu, phone: 302-831-2440; fax: 302-831-1228

2 Lecturer, Water Research Laboratory, School of Civil and Environmental Engineering, University of New South Wales, Sydney, NSW 2052, c.blenkinsopp@unsw.edu.au, phone +61 2 80719800; fax +61 2 99494188

3Associate Professor, Coastal Processes Research Group, School Marine Science & Engineering, Plymouth University, Room 121 Reynolds Bldg., Drake Circus, Plymouth, Devon PL4 8AA, United Kingdom, daniel.conley@plymouth.ac.uk, phone: +44 (0)1752-584561; fax +44 (0)1752-586101

4 Associate Head of School, Coastal Processes Research Group, School Marine Science & Engineering, Plymouth University, Room 115 Reynolds Bldg., Drake Circus, Plymouth, Devon PL4 8AA, United Kingdom, gerd.masselink@plymouth.ac.uk, phone: +44 (0)1752-585902; fax +44 (0)1752-586103

5 Associate Professor, Water Research Laboratory, School of Civil and Environmental Engineering, University of New South Wales, Sydney, NSW 2052, ian.turner@unsw.edu.au, phone +61 2 80719829; fax +61 2 99494188

6 Professor, Coastal Processes Research Group, School Marine Science & Engineering, Plymouth University, Room 114 Reynolds Bldg., Drake Circus, Plymouth, Devon PL4 8AA, United Kingdom, P.Russell@plymouth.ac.uk, phone: +44 (0)1752-58584741; fax +44 (0)1752-584710

7 Post-Doctoral Researcher, Coastal Processes Research Group, School Marine Science & Engineering, Plymouth University, Room 119 Reynolds Bldg., Drake Circus, Plymouth, Devon PL4 8AA, United Kingdom, Daniel.buscombe@plymouth.ac.uk, phone: +44 (0)1752-58586143; fax +44 (0)1752-584710

8 Graduate Research Assistant, Water Research Laboratory, School of Civil and Environmental Engineering, University of New South Wales, Sydney, NSW 2052, daniel.howe@unsw.edu.au, phone +61 2 80719800; fax +61 2 99494188

9 Graduate Research Assistant, Center for Applied Coastal Research, Ocean Engineering Bldg., University of Delaware, Newark, DE 19716, thijs@udel.edu, phone: 302-831-6550; fax: 302-831-1228

10 Graduate Research Assistant, Coastal Processes Research Group, School Marine Science & Engineering, Plymouth University, Room 119 Reynolds Bldg., Drake Circus, Plymouth, Devon PL4 8AA, United Kingdom, Robert.mccall@plymouth.ac.uk, phone: +44 (0)1752-58586181; fax +44 (0)1752-554719

11 Post-Doctoral Researcher, Coastal Processes Research Group, School Marine Science & Engineering, Plymouth University, Room 119 Reynolds Bldg., Drake Circus, Plymouth, Devon PL4 8AA, United Kingdom, Timothy.Poate@plymouth.ac.uk, phone: +44 (0)1752-58586181; fax +44 (0)1752-554719

Journal of Waterway, Port, Coastal, and Ocean Engineering. Submitted November 29, 2012; accepted May 2, 2013; posted ahead of print May 4, 2013. doi:10.1061/(ASCE)WW.1943-5460.0000210

Keywords: Beach erosion, Suspended load, Sheet flow, Beach face

Abstract: A comprehensive study of swash-zone hydrodynamics and sediment transport was conducted on a macrotidal beach in Perranporth, United Kingdom. The unique study is the first to simultaneously measure suspended sediment and sheet flow sediment concentrations, water depth, near-bed velocity profiles and high resolution swash surface and bed-level changes on a natural beach. Data collected during the study are used to quantify the vertical profile of cross-shore and alongshore velocities and the importance of sheet flow sediment processes in the swash zone. The swash-zone boundary layer for cross-shore velocities is observed to generally occur over at least the lower 0.06 m of the water column. Alongshore velocities are often the same order of magnitude as the cross-shore velocities and are dominant near cross-shore flow reversal. Flows are often logarithmic in profile, but the instantaneous nature of the measurements renders application of the logarithmic model difficult. When valid, the logarithmic model enabled cross-shore shear stress estimates of up to 21.8 N m^{-2} with maximum alongshore shear stress estimates of 12.3 N m^{-2}; further highlighting the potential importance of alongshore flows. Friction coefficient estimates, assuming a quadratic drag law, showed no statistical difference between onshore- and offshore-directed motion with typical values of 0.023 ± 0.013 (mean ± standard deviation). Sheet flow concentrations exceeded the maximum measured suspended sediment concentrations of approximately 400 kg m^{-3}. Sediment loads in the sheet layer are up to 10 times larger than the sediment loads in the lower suspension layer. Simplified sheet flow sediment transport estimates are 3.6 times larger on average than those in the suspension layer. The latter two findings indicate the importance of sheet flow processes in the swash zone that are generally ignored.

Journal of Waterway, Port, Coastal, and Ocean Engineering. Submitted November 29, 2012; accepted May 2, 2013; posted ahead of print May 4, 2013. doi:10.1061/(ASCE)WW.1943-5460.0000210

Introduction

Quantification of hydrodynamic and morphodynamic processes occurring across a range of spatial and temporal scales is needed to understand nearshore sediment transport. The swash zone, where wave-driven flows alternately wash up and down the beach face, is one area of the nearshore where sediment transport understanding and prediction is particularly difficult. Rapid, turbulent, shallow ephemeral flows with large sediment loads hamper in situ velocity and sediment transport measurements.

Swash-zone sediment transport is generally studied using current meters and optical backscatter sensors (e.g. Alsina and Caceres, 2011; Butt and Russell, 1999; Masselink *et al.*, 2005; Puleo *et al.*, 2000) that are designed for suspended load supported by turbulent fluctuations. The product of the velocity and concentration measurement is used to determine sediment transport at a given elevation above the bed. Improved vertical resolution is attainable with an array of optical backscatter sensors (OBS), but their size, even though small, often precludes their use in this way for swash-zone flows. Instead, fiber or miniature optic backscatter sensors (FOBS or MOBS) are used because the sensor size and sampling volume are smaller, enabling a sediment concentration profile at up to 0.01 m resolution to be obtained (Butt *et al.*, 2009; Puleo, 2009; Puleo *et al.*, 2000). FOBS/MOBS data have provided improved insight into the suspended sediment transport processes that occur in the swash zone such as the variability in elevation and duration of the suspension peaks during uprush and backwash. However, neither OBS nor FOBS/MOBS provide any information on sediment transport processes that occur within the bed. Swash-zone sediment transport also contains a bedload or sheet flow component of unknown magnitude in relation to sediment fluxes higher in the water column. Past research

Journal of Waterway, Port, Coastal, and Ocean Engineering. Submitted November 29, 2012; accepted May 2, 2013; posted ahead of print May 4, 2013. doi:10.1061/(ASCE)WW.1943-5460.0000210

focused on integrated transport suggested the potential importance of near-bed sediment transport (Horn and Mason, 1994) and other limited in situ data (Yu *et al.*, 1990) has indicated the magnitude of the near-bed sediment concentration signal. New sensors have been designed recently (Lanckriet *et al.*, 2013; Lanckriet *et al.*, this issue) that now enable quantification of the vertical profile of sediment concentration in the sheet flow layer. Gradients in the total load transport (bedload plus suspended load), regardless of the dominant transport mode, drive small-scale morphological change on an inter-swash basis (Blenkinsopp *et al.*, 2010a) that over time can lead to significant net morphological change.

The other component of the sediment transport signal to be determined is the swash-zone velocity or other hydrodynamic descriptors that influence sediment mobilization. Swash-zone cross-shore velocities are generally measured using impeller (Puleo *et al.*, 2000), electromagnetic (Masselink *et al.*, 2005) or Acoustic Doppler Velocimeters (ADVs; Raubenheimer, 2002). Typical impellors have a diameter that does not allow for measurements in close proximity to the bed. The other two sensor types have a smaller measuring volume and can be located within just a few centimeters of the bed. Due to their size and/or measuring characteristics, only several of these sensors can be deployed at a particular location to measure the vertical distribution of swash-zone velocity. More recently, a miniature pulse-coherent acoustic Doppler current profiler (PC-ADCP) has been used to quantify the vertical distribution of the near-bed velocity at high spatial resolution (0.001 m) under benign forcing conditions (Puleo *et al.*, 2012). Less attention has been paid to alongshore (Austin *et al.*, 2011) and vertical flows (Aagaard and Hughes, 2006) in the swash zone. Turbulence estimation in the swash zone has been largely relegated to laboratory (Cowen *et al.*, 2003; Petti and Longo, 2001) or numerical model studies

Journal of Waterway, Port, Coastal, and Ocean Engineering. Submitted November 29, 2012; accepted May 2, 2013; posted ahead of print May 4, 2013. doi:10.1061/(ASCE)WW.1943-5460.0000210

(Zhang and Liu, 2008). However, Aagaard and Hughes (2006) did estimate swash-zone turbulence under natural swash conditions using the vertical velocity component.

Some difficulties with measuring shallow-water swash flows are evident from a time series description of water depth and velocity from a single swash cycle (Figure 1). Even the definition of a swash cycle itself can be misconstrued depending on the application. The typical approach is to study a swash event, rather than a full cycle at a given cross-shore location. An event is typically identified by the submergence or emergence of a current meter some elevation above the bed. In field applications, the elevation of the lowest current meter (Z_{cm} in Figure 1) is generally in the range 0.01 to 0.04 m, with 0.03 - 0.04 m being most common. At a particular cross-shore location, there may be short-lived onshore-directed motion for water depths shallower than Z_{cm}, or the initial velocity data are removed in quality control procedures, eliminating some of the uprush motion from the record artificially. This removal usually results from initial submergence of an electromagnetic current meter or bubble interference with acoustic sensors. During offshore-directed motion, the backwash is also artificially truncated as the accelerating and thinning flow passes below the elevated current meter. Difficulties with swash event definition occur in *every* study that uses an elevated current meter to define swash initiation and termination. Newer remote sensing techniques such as ultrasonic distance meters (Turner *et al.*, 2008) and LiDAR (Blenkinsopp *et al.*, 2010a) enable measurement of the cross-shore distribution of free surface elevation for the entire swash cycle. Data are used to infer the depth-averaged velocity via volume continuity techniques (Blenkinsopp *et al.*, 2010b) that partially alleviates the duration issue associated with current-meter-signal-defined swash events.

Journal of Waterway, Port, Coastal, and Ocean Engineering. Submitted November 29, 2012; accepted May 2, 2013; posted ahead of print May 4, 2013. doi:10.1061/(ASCE)WW.1943-5460.0000210

Knowledge of the flow field in direct vicinity of the bed under field conditions is unknown regardless of the location of the lowest current meter or the use of newer remote sensing techniques. Flows in this region within 0.01-0.4 m of the bed level are generally assumed to be depth-uniform using the value from the current meter (e.g. Puleo *et al.*, 2000) or some profile such as a logarithmic law (Raubenheimer *et al.*, 2004) is applied. Recent velocity profile measurements on a moderately steep, microtidal, low energy beach indicated the existence of this logarithmic layer in the lower 0.03 m of the water column (Puleo *et al.*, 2012) for ensemble-averaged swash motions. Yet, detailed knowledge of the shape of the near-bed velocity profile under more energetic, low sloping, macrotidal beaches is not known.

The 1st International Workshop on Swash-Zone Processes (Puleo and Butt, 2006), convened in 2004, identified the numerous deficiencies described above. As a culmination of the collaborative efforts initiated during the workshop, a unique Beach Sediment Transport (BeST) study that simultaneously measured instantaneous water depth, velocity profiles, turbulent kinetic energy, sediment concentration from the at-rest bed up through the lower water column and inter-swash morphological change was conducted in October 2011 to address some of these key swash-zone processes. The main objectives for conducting the experiment include: a) quantifying sheet flow transport in the swash zone, b) understanding the relative importance between suspended sediment transport and sediment transport within the highly-concentrated sheet flow layer, c) the role of turbulence and dissipation in mobilizing sediment, d) the cross-shore and vertical distribution of turbulence within the swash zone and e) the ability to extract relevant hydrodynamic parameters from remote sensing methodologies such as LiDAR. Part 1 describes the overall framework for the field study and presents an overview of initial

Journal of Waterway, Port, Coastal, and Ocean Engineering. Submitted November 29, 2012; accepted May 2, 2013; posted ahead of print May 4, 2013. doi:10.1061/(ASCE)WW.1943-5460.0000210

hydrodynamic, morphodynamic and sediment concentration results obtained. Future papers will focus on the aforementioned individual aspects in more detail with the Part 2 companion paper (Lanckriet et al., this issue) addressing sheet flow transport during backwash. .

Field Site, Sensor Deployment and Data Reduction

Site Location and Hydrodynamic Conditions

The BeST field study occurred from 9-15 October, 2011 on Perran Beach in Perranporth, Cornwall, United Kingdom (Figure 2). Perran Beach is a low-gradient macrotidal beach with a mean tidal range of 5.43 m. The shoreline orientation is approximately north-south and is bound by Droskyn and Ligger Points, respectively. Measurements during the BeST campaign were collected around high tide, with durations of 3-4 hours, for 10 consecutive tidal cycles across a spring tide sequence (Figure 3, grey shaded regions). Figure 3A shows the predicted tidal level during this period. These particular tidal sequences were chosen because the high tides were all centered around 3 m Ordnance Datum Newlyn (ODN). The significant wave height (Figure 3B) and spectral peak period (Figure 3C) were measured in approximately 10 m water depth by a Datawell Directional Waverider buoy (50° 21' 11.34' ' N, 5° 10' 30.11' ' W; Channel Coastal Observatory; www.channelcoast.org). Significant wave height at the beginning of the study exceeded 2.5 m and decreased over the remaining tidal cycles to around 0.5 m during the last high tide observed. The spectral peak period was approximately 10 s for the first 4 tidal cycles before increasing to 15 s before the 5th tidal cycle. The spectral peak period then decreased over the remainder of the experiment until it was again nearly 10 s during the last tidal cycle. The offshore peak wave direction varied by up to 30° relative to shore normal (the dashed horizontal line in Figure 3D). Wave direction shows variability throughout the tidal cycle

Journal of Waterway, Port, Coastal, and Ocean Engineering. Submitted November 29, 2012; accepted May 2, 2013; posted ahead of print May 4, 2013. doi:10.1061/(ASCE)WW.1943-5460.0000210

implying that tidal effects at the location of the buoy play an important role in the depth influence on wave refraction. However, the wave obliquity in the surf and swash zones did not seem to exhibit this much spread about shore normal.

Sensor Deployment

A 45 m long scaffold frame was installed near the high tide line for mounting sensors (Figure 4A). A local right-handed coordinate system was established with cross-shore distance, x, increasing onshore and alongshore distance, y, increasing to the north. Forty-five ultrasonic distance meters (UDM; Massa M300/95) were installed at an elevation approximately 1 m above the bed at one meter intervals spanning the length of the frame. Each UDM measures the free surface when the area below it is immersed or the sand elevation when the area below it is exposed. Thus, the sensors can be used to obtain cross-shore time series of water depth and morphological change in the swash zone (Turner *et al.*, 2008). UDMs were sampled at 4 Hz. A SiCK LiDAR line scanner (SiCK LMS511) was erected on a scaffold pole at an elevation of 5 m above the bed to obtain complimentary measurements to the ultrasonic distance meters (Blenkinsopp *et al.*, 2010a). The line scanner is more highly resolved in the cross-shore than UDMs with an angular resolution of 0.25° leading to a cross-shore spatial resolution of 0.025 m near the scanner and 0.2 to 0.4 m near the landward and seaward ends of the scaffold frame respectively. The line scanner was sampled at 35 Hz. A near-bed pressure sensor (Druck PTX1830) for measuring forcing conditions was deployed 5 m seaward of the offshore end of the scaffold frame and sampled at 4 Hz.

Journal of Waterway, Port, Coastal, and Ocean Engineering. Submitted November 29, 2012; accepted May 2, 2013; posted ahead of print May 4, 2013. doi:10.1061/(ASCE)WW.1943-5460.0000210

Other swash-zone measurements were largely concentrated on a main instrument bar of the scaffold frame (Figure 4A), spanning 2 m in the alongshore (Figure 4B) and located near the mean high water line. Cross-shore and alongshore velocities (u,v respectively) were recorded by two Valeport electromagnetic current meters (EMCM) positioned nominally at 0.03 m and 0.06 m above the bed (sensors denoted by "a" in Figure 4B). The cross-shore distribution of velocity and turbulence was recorded with 3 Nortek Vectrino I acoustic velocimeters (sensors denoted by "b" in Figure 4B). Each sensor measures the three velocity components (u,v,w, where w is the vertical velocity) at nominally 0.05 m above the bed. One Vectrino I was located on the main instrument bar with another located 1.5 m seaward (Figure 4B) and the other 1.5 m landward (not visible in Figure 4B). Vectrino I sensors were sampled at 100 Hz. Highly-resolved near-bed velocity profiles (u,v,w) were recorded with 3 Vectrino II acoustic Doppler current profilers (PC-ADCP; sensors denoted by "c" in Figure 4B). The PC-ADCPs record the velocity profile at 0.001 m vertical bin spacing over a range of 0.03 m. The lowest PC-ADCP was initially deployed so the lower 0.01 m of the profiling range was located within the bed. The additional PC-ADCPs were deployed with alongshore offsets of 0.2 m and vertical offsets of 0.025 m. The PC-ADCP arrangement nominally provides the velocity profile from the bed level to around 0.07 m above the bed at 0.001 m increments. It is believed that this is the first time velocity profiles in the swash-zone boundary layer of a macrotidal beach have been recorded at this resolution. Other work has used a single Vectrino II on a microtidal beach to investigate near-bed swash-zone flows (Puleo *et al.*, 2012). The PC-ADCPs were sampled at 100 Hz. The main instrument bar contained a co-located UDM and also 2 buried pressure transducers (Figure 4B; Druck PTX1830). Buried pressure transducers were offset by 0.04 m in the vertical and the upper sensor was initially deployed 0.05 m below the bed. Pressure transducers were used to estimate

Journal of Waterway, Port, Coastal, and Ocean Engineering. Submitted November 29, 2012; accepted May 2, 2013; posted ahead of print May 4, 2013. doi:10.1061/(ASCE)WW.1943-5460.0000210

infiltration rates and determine water depth, *h*, after accounting for the sensor distance below the bed.

Two different sensors were used to measure sediment concentration. Suspended sediment concentration (SSC) was recorded using a newly constructed FOBS. This version of the FOBS consists of two separate probes (sensors denoted by "d" in Figure 4B). The lower probe contains 10 fiber optic send-receive pairs separated by 0.01 m in the vertical. The lower 3 pairs are initially buried to enable data capture under mildly erosive conditions. The upper 10 pairs have vertical spacing of 0.01, 0.02, 0.03, 0.03, 0.04, 0.05, 0.06, 0.06, 0.06, 0.07 m. Only channels 1, 2, 4, 6, and 9 were functioning during this study. The FOBS was sampled at 4 Hz. Sediment concentrations near the bed and in the sheet flow layer were measured using a conductivity concentration profiler (CCP; for a full description see Lanckriet *et al.*, 2013; Lanckriet *et al.*, this issue). The CCP is a new sensor that uses conductivity as a proxy for sediment concentration. Fresh and salt water both have conductivities several orders of magnitude higher than the essentially non-conductive sand. Thus, when sand is present within a particular measurement volume, the conductivity of that volume will decrease relative to the sand/water ratio. Using conductivity as a proxy for sheet flow sediment concentration (SFSC) is not new (Horikawa *et al.*, 1982; Ribberink and Al-Salem, 1995) because other techniques such as optical backscatter are not appropriate under these high concentration scenarios. Previous field studies that used conductivity to measure SFSC provided data at only a single elevation (Yu *et al.*, 1990). The new CCP profiles the SFSC with 0.001 m vertical resolution over a range of 0.29 m. The CCP consists of a removable probe with gold-plated electrodes and a PVC housing containing the electronics. The sensing mechanism relies on the 4-electrode approach (Li and Meijer, 2005)

Journal of Waterway, Port, Coastal, and Ocean Engineering. Submitted November 29, 2012; accepted May 2, 2013; posted ahead of print May 4, 2013. doi:10.1061/(ASCE)WW.1943-5460.0000210

and circuitry within the housing multiplexes through the electrode array to return the SFSC profile. Sensors were deployed by burial with only the small measurement portion with cross-sectional area of 0.0016 m (thick) x 0.0056 m (wide) x ~ 0.04 m (high) exposed to the flow. Sensor burial reduces scour and wake effects and the surrounding sand helps support the thin, semi-flexible probe tip. Three CCPs (sensors denoted by "e" in Figure 4B) were deployed under the main instrument bar with alongshore separation of approximately 0.2 m and vertically separated to obtain a larger profile of the SFSC. During deployment, sensors were aligned by eye such that the electrodes were parallel to the cross-shore direction to reduce wake effects and scour. CCPs were sampled at 4 Hz.

A 4 m aluminium tower was erected in the dunes landward of the scaffold frame to mount several cameras. A Sony DFW-X710 IEEE1394 protocol (firewire) visible-band, red-green-blue (RGB) camera with a 1024 x 768 pixel array sampled 5-minute image sequences at 5 Hz every 15 – 30 minutes during daylight hours when the swash-zone sensors were actively recording. A FLIR thermal infrared camera with a 640 x 480 uncooled microbolometer sensitive in the 7-14 μm band sampled 5-minute image sequences at 6.25 Hz every 15 – 30 minutes when the swash-zone sensors were actively recording during both daylight and darkness. Finally, a miniature, downward-looking, visible-band in-situ bed camera (IBC) with a 720 x 576 pixel array was deployed from the instrument bar to identify: 1) temporal phases of the swash cycle when bedload or sheet flow occurred, and 2) the instant when sediment mobility ceased during the bed settling process when only a thin sheet of water remains on the beach face at the end stages of backwash. Additionally, the IBC was used to confirm the correct cross-shore orientation of the CCP sensors, and to confirm that the potential wake effects and scour due to incorrect alignment

Journal of Waterway, Port, Coastal, and Ocean Engineering. Submitted November 29, 2012; accepted May 2, 2013; posted ahead of print May 4, 2013. doi:10.1061/(ASCE)WW.1943-5460.0000210

were minimal. The IBC was sampled at 8 Hz. Imagery results from the BeST study are not analyzed in this paper.

All sensors were surveyed into the local coordinate system using an electronic total station. The beach profile down the center of the scaffold frame and 25 m either side of the frame was measured before and after each tide. Beach profiles measured prior to high tide 7 on 13 October 2011 are shown in Figure 5A. The main instrument bar was located near the mean high water (MHW) line at a cross-shore location of x = - 68.4 m (black square in Figure 5A). The scaffold frame extended from x = - 74.8 to x= - 30.7 m (horizontal extent shown in Figure 5A). Beach profiles show little alongshore variation and the slope near MHW is roughly 1:45 for all three profiles. Surface sediment samples were collected along the central profile from x = -75.7 to -29.0 m at ~1 m intervals. The median grain size, D_{50}, was determined using a settling tube. D_{50} for Perran Beach near the main instrument bar is 0.33 mm, but shows a slight coarsening trend with increasing onshore distance (Figure 5B).

All sensors on the scaffold frame and the RGB and thermal cameras were cabled into a shore-based cabin for power, control and data acquisition. The numerous sensors and cameras were recorded on individual laptop computers. Time synchronization between sensing systems was achieved using GPS time standard (Coordinated Universal Time; UTC) and Network Time Protocol (NTP) NetTime software. One laptop computer served as the master time server with other laptops receiving the time code either via wired or wireless connection. Each laptop updated its internal clock every second with the master time server to avoid clock drift.

Journal of Waterway, Port, Coastal, and Ocean Engineering. Submitted November 29, 2012; accepted May 2, 2013; posted ahead of print May 4, 2013. doi:10.1061/(ASCE)WW.1943-5460.0000210

The elevation above the bed for sensors on the main instrument bar was measured before and following each tide. Sensor elevation is assumed to vary linearly over the tidal cycle based on these pre- and post-tide measurements since sensor elevation relative to water depth is used for quality control purposes (see below). Vertical adjustments were made prior to the subsequent tide, as necessary, to return sensors to their planned elevations.

Sensor Calibration and Data Quality Control

Pressure transducer data were corrected for atmospheric pressure and converted to water depth using gains and offsets determined by a dedicated laboratory pressure calibration facility. The EMCM and PC-ADCP sensors used in this study were calibrated by their manufacturers and are highly stable. CCP data were converted to sediment concentration using Archie's Law (Archie, 1942) and the clear-water and packed bed sediment conductivities (Lanckriet *et al.*, 2013). FOBS data were calibrated in the laboratory by adding known sediment masses in incremental amounts to a recirculation chamber with a known volume of fluid. Individual FOBS channels were set to saturate at 400 kg m^{-3}. UDM data were corrected to take into account sound speed variation in air with temperature using air temperature recorded at the cross-shore scaffold rig by a Lacrosse weather station. The LiDAR returned the local polar coordinates (distance and angle) of 761 points within the 190° field of view. The polar coordinates were first transformed to a standard Cartesian coordinate system. Coordinates were subsequently transformed to the local coordinate system using a resection based on the surveyed position of 3 fixed control points located within the LiDAR field of view.

Journal of Waterway, Port, Coastal, and Ocean Engineering. Submitted November 29, 2012; accepted May 2, 2013; posted ahead of print May 4, 2013. doi:10.1061/(ASCE)WW.1943-5460.0000210

Water depths from the PTs were corrected to account for elevation change measurements made pre- and post-tide. UDM water depths were quantified by subtracting the most recent measured bed elevation from UDM data when the bed was exposed (Turner *et al.*, 2008). UDM data were removed from the record when the sensor was submerged, had a signal return smaller than 50% or when the distance between the sensor face and water level was smaller than the instrument minimum sensing range of 0.3 m. EMCM and PC-ADCP data were removed from the record when the water depth identified by the PT was less than the sensor elevation. PC-ADCP data were removed when the beam correlation was less than 60 % or the beam amplitudes of at least 2 beams were less than -30 dB (similar to the approach used by Puleo *et al.* (2012) with these sensors). Poor correlation and weak amplitude is usual associated with bubbles or a large sediment load within the sampling volume. Additionally, PC-ADCP data were removed if 1) velocity differences of greater than 0.5 m s^{-1} were recorded between subsequent measurements (corresponding to a clearly erroneous measured flow acceleration of 50 m s^{-2}) or 2) if any remaining velocity measurements occurred for time segments of less than 6 samples. The bed level for the lowest PC-ADCP was determined using the mean and standard deviation of the velocity profile (Puleo *et al.*, 2012) over a 5 s time duration. The highest bin from the lowest PC-ADCP where the mean velocity magnitude and standard deviation were both less than 0.05 m s^{-1} was deemed the bed location. Data below the bed were discarded and profiles where no bed was identified were not used in the analysis. Bin elevations for the other PC-ADCPs were adjusted accordingly using the known vertical offset of 0.025 m between sensors. FOBS and CCP data were discarded when particular channels were located above the instantaneous water level. Additionally, CCP data were removed from the record when the sheet thickness was less than a cutoff of 0.005 m as this was the minimum sheet thickness that can be resolved by the

Journal of Waterway, Port, Coastal, and Ocean Engineering. Submitted November 29, 2012; accepted May 2, 2013; posted ahead of print May 4, 2013. doi:10.1061/(ASCE)WW.1943-5460.0000210

CCP (Lanckriet *et al.*, this issue) or the flow incidence angle was greater than 15º. Large incidence angles could cause eddy shedding behind the CCP that can elevate sheet flow concentrations. Only CCP data from one sensor with the greatest coverage of the sheet layer are used here. Data from the study during a representative one-hour long segment of the ebbing portion of tide 7 on 13 October 2011 are presented in the following sections to briefly illustrate a number of the swash-zone phenomena that this unique dataset is now being employed to investigate in further detail.

RESULTS

Beach Profile Variability

Temporal sampling of the beach profile shows a consistent steepening of the landward portion of the beach face throughout the experiment (Figure 6A). The cumulative elevation change indicates erosion of the order of 0.1 m seaward of the main instrument bar (the white dashed line in Figure 6B). Corresponding accretion of ~ 0.1 m is observed near the landward end of the scaffold frame where the landward and seaward ends of the scaffold frame are identified by the horizontal dashed black lines. Cross-sectional area changes based on pre- and post-tide centreline cross-shore profile surveys are integrated across the profile and used to infer the net cumulative sediment flux per beach width required to cause the observed profile change. Cumulative sediment flux estimates vary from about 0.5 m^2 to 1.2 m^2 (Figure 6C). There is a flux increase in association with the increase in wave period around high tides 6 and 7 even though the significant wave height is smaller than earlier in the study period.

Journal of Waterway, Port, Coastal, and Ocean Engineering. Submitted November 29, 2012; accepted May 2, 2013; posted ahead of print May 4, 2013. doi:10.1061/(ASCE)WW.1943-5460.0000210

Velocity Profiles, Logarithmic Law and Bed Shear Stress

Example cross-shore and alongshore velocity time series from elevations up to 0.065 m above the bed are shown in Figure 7. Cross-shore velocity magnitudes exceed 2 m s^{-1} (Figure 7A) whereas alongshore velocity magnitudes exceed 1 m s^{-1} (Figure 7B). Color shading of the different time series is related to the approximate elevation above the bed with the vertical separation indicating variability in boundary layer thickness. Only velocities from several elevations out of the greater than 70 non-overlapping PC-ADCP bins are shown. Cross-shore velocity variability in the vertical direction is clearly evident at up to 0.065 m above the bed with variations depending on flow phase. For example, a long duration offshore-directed flow begins near 17:41:55. The flow is nearly depth uniform during the initial stages following flow reversal as evidenced by the small vertical separation of the time series. However, vertical separation of the velocity magnitudes resulting from boundary layer growth becomes apparent as the flow duration increases. For the time segment shown, the boundary layer, again depicted by the vertical separation of the time series, is not as evident during the onshore-directed flow (roughly 17:41:30:17:41:55 in Figure 7A).

In general the alongshore velocity time series do not exhibit as clear a boundary layer structure (Figure 7B) despite the presence of vertical separation of velocity magnitude in the time series. Alongshore velocities show a dominance of southerly flow during this time period. Alongshore flow does contain direction reversals though, for example just after 17:41:30 and again near 17:42:22 in Figure 7B on timescales consistent with infragravity motions. The data gaps in both

Journal of Waterway, Port, Coastal, and Ocean Engineering. Submitted November 29, 2012; accepted May 2, 2013; posted ahead of print May 4, 2013. doi:10.1061/(ASCE)WW.1943-5460.0000210

time series result from the quality control procedures applied previously and in this case likely stem from sensor emergence and bubbles upon bore arrival at the sensor location.

Boundary layer structure is more apparent when individual velocity profiles are plotted as a function of elevation (Figure 8). Figure 8A shows the water depth for the infragravity event depicted in Figure 8. The event exceeds 60 s in duration with a maximum water depth of 0.68 m and is preceded and followed by a nearly exposed bed. Corresponding cross-shore (black) and alongshore (gray) velocity time series from roughly 0.02 m above the bed are shown in Figure 8B. Cross-shore and alongshore velocity profiles from the 3 PC-ADCPs are plotted in Figures 8C and 8D respectively with the temporal sampling location identified by the vertical colored lines in Figure 8B. The highest magnitude offshore-directed flow (red curve) exceeds 2 m s^{-1} near the bed with smaller velocities higher in the water column. The three curve segments indicate the 3 individual PC-ADCPs with all three segments showing profile curvature indicative of the expected boundary layer structure. Other offshore-directed flow instances (black, yellow, magenta curves; Figure 8) have roughly the same magnitude of 1 to 1.5 m s^{-1} and a similar velocity profile shape with smaller velocities near the bed. Cross-shore velocities during flow reversal throughout the lower water column are all near zero with no obvious near-bed phase lead observed (blue curve; Figure 8). Onshore-directed flows (green and cyan curves; Figure 8) for the two instances shown are less similar. These two instances were isolated to highlight differences in the boundary layer structure depending on swash flow conditions for roughly the same water depth. The boundary layer is more defined near 17:41:35 (green curve; Figure 8) with larger maximum onshore-directed velocities of 1.5 m s^{-1}. This velocity profile was taken roughly 10 s after uprush commencement where the water depth increased gradually. In

Journal of Waterway, Port, Coastal, and Ocean Engineering. Submitted November 29, 2012; accepted May 2, 2013; posted ahead of print May 4, 2013. doi:10.1061/(ASCE)WW.1943-5460.0000210

contrast, the boundary layer is less evolved near 17:42:35 (cyan curve; Figure 8) with maximum onshore-directed velocities of 1 m s^{-1} and smaller vertical gradients in velocity. This profile was taken roughly 5 s after uprush commencement following a rapid increase in water depth from a backwash to uprush transition.

Although often ignored in swash zone field studies, the alongshore velocity component can be significant when compared to the cross-shore velocity component especially near flow reversal (Figure 8). For example, the alongshore velocity 0.05 m above the bed exceeds 0.4 m s^{-1} when the cross-shore velocity is essentially zero. In all cases here, the alongshore velocity is directed to the south and shows a less obvious boundary layer structure. There is clearly curvature of the velocity profiles near the bed in the lower 0.02 to 0.03 m of the water column but a logarithmic model type profile structure is not as evident higher in the water column.

The mean velocity profile in a fully developed turbulent boundary layer is often quantified using the von Karman-Prandtl relationship

$$u(z) = \frac{u_*}{\kappa} ln\left(\frac{z}{z_0}\right), \quad (1)$$

where *u(z)* is the cross-shore velocity profile, u_* is the friction velocity, κ (= 0.4) is the von Karman's constant and z_0 is the roughness height. Equation (1) was not originally developed for accelerating or under-developed turbulent boundary layers, but has been used with success under

Journal of Waterway, Port, Coastal, and Ocean Engineering. Submitted November 29, 2012; accepted May 2, 2013; posted ahead of print May 4, 2013. doi:10.1061/(ASCE)WW.1943-5460.0000210

these conditions in past studies (Jensen *et al.*, 1989; O'Donoghue *et al.*, 2010; Puleo *et al.*, 2012).

The friction velocity is related to the bed shear stress as

$$\tau_x = \rho u_* |u_*|, \tag{2}$$

where ρ is the fluid density, subscript x identifies cross-shore direction and | | indicates magnitude in order to maintain the direction of cross-shore shear stress. Equations analogous to (1) and (2) exist for the alongshore velocity, $v(z)$, and bed shear stress in the alongshore direction, τ_y, in the swash zone. The total bed shear stress magnitude from cross-shore and alongshore bed shear stress components is determined as the vector resultant.

Bed shear stress calculations are generally inferred from a quadratic drag law when no velocity profile information is available as

$$\tau = \frac{1}{2}\rho f u_h |u_h|, \tag{3}$$

where f is an empirical friction factor typically O(10^{-3} to 10^{-2}) (e.g. Conley and Griffin, 2004; Puleo and Holland, 2001; Raubenheimer *et al.*, 2004) and u_h is a fluid velocity at some elevation above the bed, usually the lowest current meter, used in the calculation. When velocity profile data exist, the friction coefficient is estimated using equations 2 and 3 as

Journal of Waterway, Port, Coastal, and Ocean Engineering. Submitted November 29, 2012; accepted May 2, 2013; posted ahead of print May 4, 2013. doi:10.1061/(ASCE)WW.1943-5460.0000210

$$f = \frac{2u_* |u_*|}{u_h |u_h|} \quad .$$

(4)

The logarithmic model (Equation 1) is used to determine u_* and hence the bed shear stress. Velocity profiles are first block-averaged over 0.1 s in an effort to smooth out some of the turbulent fluctuations. A least squares regression between the velocity profile and $ln(z)$ is then performed on the profile from the lower PC-ADCP. Only the lower PC-ADCP is used in this analysis due to the alongshore separation of sensors causing potential hydrodynamic variability between measurement location (e.g. the red curve in Figure 8). The slope, s, of the least squares regression yields $u_* = s\kappa$ and the shear stress is obtained through equation (2). The square of the correlation coefficient in the regression is used to reject the logarithmic model when it poorly fits the data. Past studies using ensemble-averaged data used an r^2 cutoff of 0.9 or more (e.g. O'Donoghue *et al.*, 2010). An r^2 value that high is not appropriate in applications where ensemble-averaging is not performed and velocity fluctuations are more prevalent. Thus, an r^2 cutoff of 0.7 is used instead in this study as an indicator of poor model fit.

Cross-shore bed shear stresses vary throughout the infragravity event and range in magnitude from 0 to 6 N m^{-2} (Figure 9). There are many instances where a bed shear stress was not quantified due to poor model fit. However, when data are present, they indicate large bed shear stress even when the velocity magnitudes are not at the extremes measured during the study. In

Journal of Waterway, Port, Coastal, and Ocean Engineering. Submitted November 29, 2012; accepted May 2, 2013; posted ahead of print May 4, 2013. doi:10.1061/(ASCE)WW.1943-5460.0000210

addition, the alongshore bed shear stress τ_y (gray circles; Figure 9B) can be of similar magnitude or exceed that of τ_x (black circles; Figure 9B) even though the alongshore flow velocity is weaker than the cross-shore flow velocity. The mean of $\left|\tau_x / \tau_y\right|$ over the 6-minute duration of the data file containing this infragravity event is 3.69 suggesting that cross-shore bed shear stress is generally dominant. But the standard deviation over this short time period of the same ratio is 5.12 indicating the alongshore bed shear stress is not negligible.

The friction coefficient for cross-shore velocity profiles is determined using equation 3 and the velocity roughly 0.03 m above the bed (Figure 9C). Friction coefficients were not quantified when u_h taken at 0.03 m was less than 0.1 m s^{-1} because these small velocities squared in the denominator of equation 4 yield unrealistic values. Friction coefficients for this infragravity event range from 0.003 to 0.09 and are in the range reported previously in the literature (Conley and Griffin, 2004; Puleo and Holland, 2001; Raubenheimer *et al.*, 2004). Short-lived trends of increasing f_x occur when the cross-shore flow velocity, u_h, used in the calculation decreases. There is no statistical difference between f_x associated with onshore-directed motion ($f_x = 0.025 \pm 0.016$; mean ± standard deviation) and offshore-directed motion ($f_x = 0.021 \pm 0.012$) for the 6-minute duration of the file containing the infragravity event.

There is considerable variability in the bed shear stress and estimated friction coefficient over the course of a tide (Figure 10). The corresponding water depth (Figure 10A) reaches a maximum of 0.82 m but even near the peak tide some long duration backwash events cause the sensors to

Journal of Waterway, Port, Coastal, and Ocean Engineering. Submitted November 29, 2012; accepted May 2, 2013; posted ahead of print May 4, 2013. doi:10.1061/(ASCE)WW.1943-5460.0000210

emerge from the water column. Frequent shallow depths can hamper determination of hydrodynamic statistics. The cross-shore bed shear stress (Figure 10B) attains a maximum of 21.9 N m^{-2} whereas the maximum alongshore bed shear stress maximum is 12.3 N m^{-2} over the tidal duration. Near the beginning of the tide, the bed stress is weaker than when the sensors are more consistently submerged. This difference may be related to the transition from purely swash zone to inner surf zone processes at the cross-shore location of the measurements. Using only instances where both cross-shore and alongshore bed stress estimates were obtained, $\left|\tau_x / \tau_y\right|$ over the tide duration is 3.8 ± 6.2 (mean ± standard deviation) similar to that found for the shorter duration segment of data described previously. The friction coefficient obtained for cross-shore velocity profiles is less than 0.1 (Figure 10C) and shows no obvious trends for the tidal duration. The tidally-average friction coefficient is 0.023 ± 0.013. There is no statistical difference between f_x associated with onshore-directed motion (f_x = 0.021 ± 0.011) and offshore-directed motion (f_x = 0.025 ± 0.014) as was found for the shorter duration record presented previously (Figure 11).

Sediment Concentrations, Bed Level Variability and Sediment Loads

Bed level determination is crucial for estimating the sediment load as a function of time. Past analysis with FOBS data estimated the bed level every two minutes (Puleo *et al.*, 2000). Lanckriet *et al.* (2013) defined the bed level for CCP data as the elevation where the volumetric concentration is at a loose packing limit of 0.51 (Bagnold, 1966). However, the bed level for the

Journal of Waterway, Port, Coastal, and Ocean Engineering. Submitted November 29, 2012; accepted May 2, 2013; posted ahead of print May 4, 2013. doi:10.1061/(ASCE)WW.1943-5460.0000210

CCP data in this study is determined based on a curve fit, modified from O'Donoghue and Wright (2004), to the concentration profile. Essentially there is a sharp 'shoulder' transition region in the sheet flow concentration profile that is indicative of a volume fraction near the loose packing limit. The bottom of the sheet layer occurs near the transition region and is identified using the profile shape in a two-step procedure as described in Lanckriet *et al.* (this issue). The bed level relative to FOBS data was determined only to the nearest 0.01 m based on sensor separation of the lower section of the probe. In contrast, the bed level for the CCP was determined to the nearest 0.001 m. Thus, the exact elevation where it is assumed that no sediment is in motion will vary between the two measurement techniques.

The FOBS bed level is assumed to be located where a particular channel maintains a high concentration. A simple cutoff procedure was used to quantify the bed level location. The mean concentration for each channel over a 5 s data block was determined. The highest channel for which the mean exceeded a concentration of 160 kg m^{-3} was deemed the bed level for that duration of time. Each subsequent 5 s data block was analyzed using this approach to determine a bed level time series. Puleo *et al.* (2000) used a similar approach over a 2-minute time block and also included the standard deviation of each channel over a given time block. That approach was not necessary here given the relatively short duration of the time series and the near continual immersion in water of the sensor. Five seconds duration was deemed sufficient to identify the bed level given the FOBS vertical spacing and small observed changes in the bed level over the tidal run.

Journal of Waterway, Port, Coastal, and Ocean Engineering. Submitted November 29, 2012; accepted May 2, 2013; posted ahead of print May 4, 2013. doi:10.1061/(ASCE)WW.1943-5460.0000210

Figure 12 shows what are believed to be the first simultaneous measurements of near-bed velocity, SSC and SFSC from a natural beach. During this ~10 minute time series the water depth (Figure 12A) varies from 0 to over 0.7 m. Depths recorded by the buried PT (black), UDM (dark gray) and LiDAR (dotted black) are hard to distinguish because of their similarity indicating high correlation between the three measurements techniques for water depth for these events. The cross-shore velocity (Figure 12B; EMCM: black, PC-ADCP bin at roughly 0.03 m above bed: gray) reaches nearly 2 m s^{-1} in magnitude during onshore- and offshore-directed motions. The largest magnitude flows are observed during the latter stages of a large rundown and subsequent arrival of an incoming bore (near 17:41:10 and 17:44:10). Both sensors are capable of returning the velocity time series but the acoustic approach has more data interruptions likely due to bubbles. Figure 12C shows the SSC from the 5 FOBS channels. Time series are offset in the vertical by 400 kg m^{-3} for visual clarity. The bold segments of FOBS time series signify the bed level. FOBS data indicate three primary suspension events at roughly 17:39:24, 17:39:40 and 17:41:16. Suspension pulses often appear as double-peaked surrounding the drop in concentration between peaks occurring near flow reversal. In general, the two peaks for a given suspension event are similar in magnitude for the lower 2-3 time series. However, at times higher in the water column, SSC associated with onshore-directed motion exceeds that of the SSC associated with offshore-directed motion. Differences are likely attributed to the suspension mechanism. During onshore-directed motion, bore-generated turbulence is likely to carry sediment higher into the water column. During offshore-directed motion for these events where the water depth approaches zero, turbulence originates from the bed and eddies are constrained by the free surface. Suspension events observed in FOBS data are correlated to sediment mobilization in the sheet flow layer (Figure 12D). Nearly every other

Journal of Waterway, Port, Coastal, and Ocean Engineering. Submitted November 29, 2012; accepted May 2, 2013; posted ahead of print May 4, 2013. doi:10.1061/(ASCE)WW.1943-5460.0000210

CCP channel is shown in Figure 12D with subsequent time series offset by 1800 kg m^{-3} for visual clarity. The CCP bed location is quantified using the concentration profile and graphically displayed by the solid dots in Figure 12D. Individual channels below locations identified by the dots in Figure 12D are considered to be within the bed. The coarse spatial nature of bed identification is due to display of only a portion of the CCP channels and the lack of bed identification via the concentration profile in some measurement instances. SFSC associated with offshore- and onshore-directed motion for the primary events is generally similar in magnitude with SFSC exceeding 1000 kg m^{-3} for channels above the bed. Segments of the time series show maximum CCP concentrations followed by exposure indicating an accretion/erosion cycle on the order of 0.01 m on infragravity time scales with smaller elevation variability on incident wave time scales. Corresponding SSC data show comparatively little sediment suspended into the water column suggesting this bed level change may be more related to gradients in sheet flow transport rather than suspended sediment transport.

Sediment loads were calculated by integrating over the sediment concentration profile. SSC from FOBS data were integrated from the FOBS-defined bed level (BLF) to the highest FOBS sensor (CH5; normally 0.08 to 0.09 m above the bed) as

$$C_{SSC} = \int_{BLF}^{CH5} SSC\, dz\,. \tag{5}$$

Journal of Waterway, Port, Coastal, and Ocean Engineering. Submitted November 29, 2012; accepted May 2, 2013; posted ahead of print May 4, 2013. doi:10.1061/(ASCE)WW.1943-5460.0000210

We note that the integral for suspended load should have a lower limit at the interface between sheet flow and suspended load but the 0.01 m vertical resolution of the FOBS is not sufficient to resolve this location. Thus, the "bed level" as defined by the FOBS data is used as the lower limit. The SSC profile in the lowest 0.01 m of the water column was assumed to be uniformly distributed with a magnitude equal to the SSC at 0.01 m above the bed. There are times when the estimated bed level is located below channel 1 and its exact elevation is unknown. The bed level is assumed to occur 0.01 m below channel 1 during these instances so that a suspended load can be calculated.

SFSC from CCP data were integrated from the bed level inferred from the CCP concentration profile (BLC) up to the top of the sheet layer (SH) defined at a volumetric concentration of 0.08 (~210 kg m^{-3}) as

$$C_{SFSC} = \int_{BLC}^{SH} SFSC\, dz\,. \tag{6}$$

C_{SFSC} was not calculated if the bottom of the sheet layer was not identifiable from the record, the top of the sheet layer extended above the highest sensor electrode or the sheet layer thickness was less than 0.005 m.

Journal of Waterway, Port, Coastal, and Ocean Engineering. Submitted November 29, 2012; accepted May 2, 2013; posted ahead of print May 4, 2013. doi:10.1061/(ASCE)WW.1943-5460.0000210

Sediment load calculations exceed 4 kg m^{-2} for FOBS data and reach almost 15 kg m^{-2} for CCP data (Figure 13B). Corresponding water depth time series (Figure 13A) show that the high sediment loads occur at the offshore-to-onshore transitions when the water depths are shallow or the bed has become inundated. In all cases when data are present C_{SFSC} exceeds C_{SSC}. Unfortunately, large data gaps in CCP data occur because of conservative estimates of the bottom and top of the sheet layer and requirement for flow to be nearly shore normal. The ratio, C_{SFSC}/C_{SSC}, is always greater than 1 based on Figure 13B and is heavily influenced by small C_{SSC} values under active sheet flow but relatively little suspended load. The mean ratio over the hour-long data segment is 9.5 ± 8.4 (mean ± standard deviation) using only instances where C_{SSC} exceeds 0.2 kg m^{-2}; where a minimum C_{SSC} is used to include only times where sheet flow *and* suspended load both occur. Note, however, that these ratios do not indicate that sheet load *transport* exceeds that of suspended load transport because the velocities in the sheet layer and within the water column vary considerably.

Discussion

This paper presents an overview of a comprehensive study of swash zone sediment transport. The study is unique in that it is the believed to be the first time that field data consisting of highly-resolved near-bed velocity, water depth, inter-swash bed level changes and both sheet flow sediment and suspended sediment concentrations have been simultaneously collected. The results presented here are a preliminary analysis of the large data set and provide new insights into swash zone hydrodynamic and morphodynamic processes.

Journal of Waterway, Port, Coastal, and Ocean Engineering. Submitted November 29, 2012; accepted May 2, 2013; posted ahead of print May 4, 2013. doi:10.1061/(ASCE)WW.1943-5460.0000210

Velocity Profiles and Bed Stress

New PC-ADCPs were used to quantify the horizontal and vertical velocity components over the lower 0.07 m of the water column at 0.001 m vertical resolution at 100 Hz. Cross-shore velocities on the macrotidal beach exceeded 2 m s^{-1} and are commensurate with maximum velocities found in previous swash-zone studies (e.g. Masselink *et al.*, 2005). Alongshore velocities in the swash zone have been studied less frequently. Austin *et al.* (2011) investigated swash-zone flows on dissipative and reflective beaches. They found alongshore velocities in the swash zone to often exceed 1 m s^{-1} with maximum values being on the same order as cross-shore velocities. Similar findings are found in this study where the alongshore velocities can exceed those of the cross-shore velocities even away from times near flow reversal. Incorporating alongshore fluid motions in swash-zone studies is important because rapid alongshore velocities may still mobilize sediment and enhance sediment transport even during the cross-shore flow reversal phase when it is generally assumed that sediment transport is weak.

Several past studies obtained a coarse representation of the velocity profile (2-4 current meters; Austin *et al.*, 2011; Raubenheimer, 2002; Raubenheimer *et al.*, 2004) and were able to use that information to infer the variability in the boundary layer shape as a function of flow direction and phase. More recently, Puleo *et al.* (2012) used a single PC-ADCP on a microtidal, low energy beach to further investigate the boundary layer structure over the lower few centimeters of the water column. The logarithmic model was applied to the velocity profiles in an effort to infer the bed shear stress and the corresponding friction coefficient. In Austin *et al.* (2011) and Puleo *et al.* (2012) studies, velocity profiles were either ensemble-averaged over averaged over a

Journal of Waterway, Port, Coastal, and Ocean Engineering. Submitted November 29, 2012; accepted May 2, 2013; posted ahead of print May 4, 2013. doi:10.1061/(ASCE)WW.1943-5460.0000210

long time before application of the logarithmic model more in accordance with the assumption of a "mean" velocity profile for a developed boundary layer. Velocity profiles in this study were only averaged over 0.1 s in an effort to retain some of the bed stress temporal information, rather than using long time averages. The model skill before acceptance was necessarily reduced because more of the turbulence and sensor noise is retained in the velocity profile as the averaging window is decreased. Still, fewer bed shear stress estimates were retained. However, cross-shore bed shear stress estimates found in this study are similar to those of previous studies under different beach slopes and hydrodynamic forcing conditions (Conley and Griffin, 2004; Puleo *et al.*, 2012) but smaller than model studies over fixed, coarse granular beds (Kikkert *et al.*, 2012; O'Donoghue *et al.*, 2010). Alongshore-directed bed shear stress was also found to have magnitudes similar to those in the cross-shore direction. It is important to point out that, similar to velocities, alongshore-directed bed shear stress can be large when cross-shore flows and/or cross-shore bed shear stresses are weak. The bed shear stress is one of several processes that mobilize sediment. But the exclusion of alongshore bed shear stress, even in a solely cross-shore sediment transport model will underpredict the sediment transport and may lead to poor model skill. It is noted that vertical velocities could also play a role in enhancing bed shear stress and were not investigated in this initial analysis although data from BeST will be used in the future to determine any potential effect on bed shear stress.

Sediment Concentrations and Transport

Sediment concentration data indicated the importance and potential dominance of sheet flow concentrations relative to those higher in the water column. We are unaware of any past studies

Journal of Waterway, Port, Coastal, and Ocean Engineering. Submitted November 29, 2012; accepted May 2, 2013; posted ahead of print May 4, 2013. doi:10.1061/(ASCE)WW.1943-5460.0000210

that have investigated the instantaneous variability of SSC to SFSC although (Horn and Mason, 1994) investigated the importance of bed load transport integrated over a swash cycle using sediment traps. The suspended sediment concentration profile obtained during BeST was of lesser vertical resolution than is probably required and did not extend high into the water column. However, swash-zone suspended sediment concentrations tend to be near the bed except during bore arrival (Masselink *et al.*, 2005; Puleo *et al.*, 2000) suggesting that much of the SSC was captured. The SSC signal was not extended to the surface in the initial analysis presented here. If the SSC profile was extended assuming a linear decay in SSC to zero at the free surface, the C_{SFSC}/C_{SSC} ratio decreases by roughly 40% on average to 5.4 ± 4.4 (mean ± standard deviation). It is unlikely that the extending the SSC profile in a linear fashion to the free surface replicates accurately the true profile but the exercise does show that even a small unaccounted for suspended sediment load above the FOBS can be significant when integrated over the rest of the water column. An additional effect on the magnitude of the C_{SFSC}/C_{SSC} ratio is the FOBS bed level determination. The FOBS bed level was found to be generally located at channel 1 with occasional increases to channel 2. If a different cutoff concentration, inclusion of concentration mean and standard deviation or other algorithm was used the estimated bed level may have varied and included some of the large concentrations observed in channel 2 as SSC. For example, if the SSC peaks near 17:42:40 and 17:44:10 in Figure 12 were included in C_{SSC} the C_{SFSC}/C_{SSC} ratio would decrease suggesting improved bed level identification algorithms may be required to more fully understand the magnitude and variability of the C_{SFSC}/C_{SSC} ratio.

The finding that C_{SFSC} is generally larger on average than C_{SSC} can have important ramifications for swash-zone sediment transport estimates from in situ data since sheet flow sediment transport

Journal of Waterway, Port, Coastal, and Ocean Engineering. Submitted November 29, 2012; accepted May 2, 2013; posted ahead of print May 4, 2013. doi:10.1061/(ASCE)WW.1943-5460.0000210

is generally ignored. The data presented in this study was only for the sediment load which is not an indicator of the sediment transport until multiplied by a velocity. Simplifications can be made to obtain a gross first order estimate of the cross-shore sheet flow sediment transport rate, Q_{SF} and suspended sediment transport rate, Q_{SS}. Q_{SS} is estimated as

$$Q_{SS} = \int_{BLF}^{CH5} u_{EMCM} SSC(z)\, dz\,, \tag{7}$$

where u_{EMCM} is the cross-shore velocity from the lowest EMCM. An argument could be made for using the PC-ADCP velocity profiles but the velocity profiles higher in the water column have little curvature, the PC-ADCPs have more data interruptions than the EMCMs and using a single velocity is adequate for a first order estimate given the assumptions in this and the subsequent calculations.

The velocity profile in the sheet layer was not measured during BeST. In fact, in situ swash-zone sheet flow velocities in the field have never been measured to the authors' knowledge. However, previous studies have suggested the velocity profile in the granular sheet layer is approximately linear with a maximum velocity at the top of the sheet layer and zero velocity at the bottom of the sheet layer (Pugh and Wilson, 1999). Q_{SF} is estimated using this assumption and that the velocity at the top of the sheet layer is equal to the cross-shore velocity of the lowest EMCM as

Journal of Waterway, Port, Coastal, and Ocean Engineering. Submitted November 29, 2012; accepted May 2, 2013; posted ahead of print May 4, 2013. doi:10.1061/(ASCE)WW.1943-5460.0000210

$$Q_{SF} = \int_{BLC}^{SH} u_{EMCM} \frac{z_s}{\delta_s} SFSC(z)\, dz\,, \tag{8}$$

where δ_s is the sheet layer thickness and z_s is a vertical coordinate with $z_s = 0$ at the bottom of the sheet layer. Estimated sediment flux magnitudes exceed 4 kg m^{-1} s^{-1} for onshore-directed flow and 5 kg $m^{-1}s^{-1}$ for offshore-directed flow (Figure 13C). Q_{SF} is greater than Q_{SS} when data from both sensor types are available but little data are present during the beginning of onshore-directed flow when suspended load transport is expected to be greatest. The Q_{SF}/ Q_{SS} ratio when the C_{SSC} exceeds 0.2 kg m^{-2} reaches up to 19.7 with typical values of 3.6 ± 2.9 (mean ± standard deviation). Even though the calculations shown here required large simplifications, the limited data indicate that the instantaneous sheet flow transport in the swash zone is generally larger than the suspended load transport.

Conclusion

A comprehensive study of swash-zone sediment transport was completed on a macrotidal beach under energetic forcing conditions for 10 tidal cycles. Survey data showed vertical beach profile variability on the order of 0.1 m over the study period. Preliminary results from a representative ebbing portion of one tide were presented, primarily to indicate the uniqueness of the data set that is now available for extensive additional investigation. Velocity profiles over the lower 0.06 m of the water column indicate the boundary layer often reaches or exceeds this elevation. Comparisons between cross-shore and alongshore flow magnitudes and bed shear stresses confirmed the importance of alongshore motions in the swash zone and suggests their exclusion

Journal of Waterway, Port, Coastal, and Ocean Engineering. Submitted November 29, 2012; accepted May 2, 2013; posted ahead of print May 4, 2013. doi:10.1061/(ASCE)WW.1943-5460.0000210

in sediment transport modelling could lead to large errors. The bed level is nearly continually adjusting during active swash flows with changes on the order of 0.01 m over durations less than 60 s observed. Sheet flow sediment concentrations exceed those measured higher in the water column with sheet flow sediment loads generally exceeding suspended sediment loads by up to a factor of 10. Simple estimates of sediment transport using the measured sediment concentrations and a velocity signal suggest the near-bed sediment transport exceeds that of the suspended sediment transport on average by a factor of 3.6, although there is significant variability.

Acknowledgements

This material is based upon work supported by the National Science Foundation under Grant No. OCE-0845004. Additional support for this work was provided by the University of Delaware, the Delaware Department of Natural Resources and Environmental Control, the Award for Global Research, Internships, and Performances for Graduate Students at the University of Delaware, the Natural Environmental Research Council (Grant NE/G007543/1), an Australian Research Council Discovery Project (DP110101176), and the US-UK Fulbright Commission. The authors would like to thank B. Proença, L. Melo De Almeida, M. Sheridan, and P. Ganderton for their assistance with the field measurements. Four reviewers provided insightful comments that improved the clarity of this manuscript.

References

Aagaard, T., and Hughes, M. G. 2006, Sediment suspension and turbulence in the swash zone of dissipative beaches, Marine Geology, 228, 117-135.

Alsina, J. M., and Caceres, I. 2011, Sediment suspension events in the inner surf and

Journal of Waterway, Port, Coastal, and Ocean Engineering. Submitted November 29, 2012; accepted May 2, 2013; posted ahead of print May 4, 2013. doi:10.1061/(ASCE)WW.1943-5460.0000210

swash zone. Measurements in large-scale and high-energy wave conditions, Coastal Engineering, 58, 657-670.

Archie, G. 1942, The electrical resistivity log as an aid in determining some reservoir characteristics, Institute of Mining and Metallurgical Transactions, 14, 54-62.

Austin, M. J., Masselink, G., Russell, P., Turner, I., and Blenkinsopp, C. 2011, Alongshore fluid motions in the swash zone of a sandy and gravel beach, Coastal Engineering, 58(8), 690-705.

Bagnold, R. A. 1966, The shearing and dilatation of dry sand and the'singing'mechanism., Philosophical Transactions of the Royal Society of London. Series A, Mathematical and Physical Sciences,, 295(1442), 219-232.

Blenkinsopp, C., Mole, M. E., Turner, I. L., and Peirson, W. L. 2010a, Measurements of the time-varying profile across the swash zone using an industrial LIDAR, Coastal Engineering, 57, 1059-1065.

Blenkinsopp, C., Turner, I., Masselink, G., and Russell, P. 2010b, Validation of volume continuity method for estimation of cross-shore flow velocity, Coastal Engineering, doi:10.1016/j.coastaleng.2010.05.005.

Butt, T., and Russell, P. 1999, Suspended sediment transport mechanisms in high-energy swash, Marine Geology, 161(2-4), 361-375.

Butt, T., Tinker, J., Masselink, G., O'Hare, T. J., and Russell, P. 2009, Field observations of sediment fluxes in the inner-surf and swash zones, Journal of Coastal Research, 25(4), 991-1001.

Conley, D. C., and Griffin, J. G. 2004, Direct measurements of bed stress under swash in the field, Journal of Geophysical Research, 109, C03050, doi.10129/2003JC001899.

Journal of Waterway, Port, Coastal, and Ocean Engineering. Submitted November 29, 2012; accepted May 2, 2013; posted ahead of print May 4, 2013. doi:10.1061/(ASCE)WW.1943-5460.0000210

Cowen, E. A., Sou, I. M., Liu, P. L.-F., and Raubenheimer, B. 2003, Particle Image Velocimetry measurements within a laboratory generated swash zone, Journal of Engineering Mechanics, 129(10), 1119-1129.

Horikawa, K., Watanbe, A., and Katori, S. 1982, Sediment transport under sheet flow conditions, paper presented at 18th International Conference on Coastal Engineering, ASCE, 1335-1352 pp.

Horn, D. P., and Mason, T. 1994, Swash zone sediment transport modes, Marine Geology, 120(3-4), 309-325.

Jensen, B. L., Sumer, B. M., and Fredsoe, J. 1989, Turbulent oscillatory boundary layers at high Reynolds numbers, Journal of Fluid Mechanics, 206, 265-297.

Kikkert, G. A., O'Donoghue, T. O., Pokrajac, D., and Dodd, N. 2012, Experimental study of bore-driven swash hydrodynamics on impermeable rough slopes, Coastal Engineering, 60, 149-166.

Lanckriet, T. M., Puleo, J. A., and Waite, N. 2013, A conductivity concentration profiler for sheet flow sediment transport, IEEE Journal of Oceanic Engineering, 38(1), 55-70.

Lanckriet, T. M., Puleo, J. A., Masselink, G., Turner, I. L., Conley, D. C., Blenkinsopp, C., and Russell, P. This issue, A comprehensive field study of swash-zone processes, Part 2: Sheet flow sediment concentrations during quasi-steady backwash, Journal of Waterway Port Coastal and Ocean Engineering.

Li, X., and Meijer, G. C. M. 2005, A low-cost and accurate interface for four-electrode conductivity sensors, IEEE Transactions on Instrumentation and Measurement, 54, 2433-2437.

Journal of Waterway, Port, Coastal, and Ocean Engineering. Submitted November 29, 2012; accepted May 2, 2013; posted ahead of print May 4, 2013. doi:10.1061/(ASCE)WW.1943-5460.0000210

Masselink, G., Evans, D., Hughes, M. G., and Russell, P. 2005, Suspended sediment transport in the swash zone of a dissipative beach, Marine Geology(216), 169-189.

O'Donoghue, T., and Wright, S. 2004, Concentrations in oscillatory sheet flow for well sorted and graded sands, Coastal Engineering, 50, 117-138.

O'Donoghue, T. O., Pokrajac, D., and Hondebrink, L. J. 2010, Laboratory and numerical study of dam-break-generated swash on impermeable slopes, Coastal Engineering, 57(5), 513-530.

Petti, M., and Longo, S. 2001, Turbulence experiments in the swash zone, Coastal Engineering, 43(1), 1-24.

Pugh, F. J., and Wilson, K. C. 1999, Velocity and concentration distributions in sheet flow above plane beds, Journal of Hydraulic Engineering, 125, 117-125.

Puleo, J. A. 2009, Tidal variability of swash-zone sediment suspension and transport, Journal of Coastal Research, 25, 937-948.

Puleo, J. A., and Holland, K. T. 2001, Estimating swash zone friction coefficients on a sandy beach, Coastal Engineering, 43(1), 25-40.

Puleo, J. A., and Butt, T. 2006, The 1st international workshop on swash-zone processes, Continental Shelf Research, 26, 556-560.

Puleo, J. A., Lanckriet, T. M., and Wang, P. 2012, Nearbed cross-shore velocity profiles, bed shear stress and friction on the foreshore of a microtidal beach, Coastal Engineering, 68, 6-16.

Puleo, J. A., Beach, R. A., Holman, R. A., and Allen, J. S. 2000, Swash zone sediment suspension and transport and the importance of bore-generated turbulence, Journal of Geophysical Research, 105(C7), 17021-17044.

Journal of Waterway, Port, Coastal, and Ocean Engineering. Submitted November 29, 2012; accepted May 2, 2013; posted ahead of print May 4, 2013. doi:10.1061/(ASCE)WW.1943-5460.0000210

Raubenheimer, B. 2002, Observations and predictions of fluid velocities in the surf and swash zones, Journal of Geophysical Research, 107(C11, 3190, doi:10.1029/2001JC001264).

Raubenheimer, B., Elgar, S., and Guza, R. T. 2004, Observations of swash zone velocities: A note on friction coefficients, Journal of Geophysical Research, 109, C01027, doi:01010.01029/02003JC001877.

Ribberink, J. S., and Al-Salem, A. A. 1995, Sheet flow and suspension in oscillatory boundary layers, Coastal Engineering, 25, 205-225.

Turner, I., Russell, P., and Butt, T. 2008, Measurement of wave-by-wave bed-levels in the swash zone, Coastal Engineering, 55, 1237-1242.

Yu, Z., Niemeyer, H. D., and Bakker, W. T. 1990, Site investigation on sand concentration in the sheet flow layer, ASCE, New York, 2360-2371 pp.

Zhang, Q., and Liu, P. L.-F. 2008, A numerical study of swash flows generated by bores, Coastal Engineering, 55, 1113-1134.

Journal of Waterway, Port, Coastal, and Ocean Engineering. Submitted November 29, 2012; accepted May 2, 2013; posted ahead of print May 4, 2013. doi:10.1061/(ASCE)WW.1943-5460.0000210

Figure Captions

Figure 1. Schematic of a swash cycle and event for water depth (top) and near bed velocity (bottom).

Figure 2. Location of Perran Beach UK (modified from Masselink et al., 2005) showing the study area.

Figure 3. Forcing conditions for the BeST field study. A) Tide level, B) Significant wave height, C) Spectral peak period and D) wave direction. Horizontal dashed line is shore normal incidence. Grey shading in all plots indicates the sampling period and tide number denoted by values on the upper axis of (A). The darker shaded region is tide 7, the ebbing portion of which is analysed in this paper.

Figure 4. Images showing the scaffold frame (A) and the main instrument bar (B). Sensors on the main instrument bar are: electromagnetic current meters (a), Vectrino I velocimeters (b), Vectrino II acoustic Doppler current profilers (c), FOBS (d) and CCPs (e). The buried pressure transducers (PTs) are only identified by their name in the image.

Figure 5. A) Beach profiles measured prior to high tide 7 on 13 October 2011 along the central, north and south transects. The horizontal dotted line identifies the mean high water (MHW) level. The solid gray horizontal line indicates the cross-shore extent of the scaffold rig and the

Journal of Waterway, Port, Coastal, and Ocean Engineering. Submitted November 29, 2012; accepted May 2, 2013; posted ahead of print May 4, 2013. doi:10.1061/(ASCE)WW.1943-5460.0000210

black square the cross-shore location of the main instrument bar. B) Median grain size within the extent of the scaffold rig as a function of cross-shore distance.

Figure 6. Morphological variability during the BeST field study. A) Cumulative elevation change for each tide. Horizontal black lines denote seaward and landward edges of the scaffold frame. Horizontal white line indicates the location of the main instrument bar. B) Cumulative volumetric flux required to cause measured elevation changes determined from pre- and post-tide beach profiles surveys.

Figure 7. Cross-shore (A) and alongshore (B) velocity time series from the ebbing portion of tide 7. Individual colors indicate the approximate elevation where the time series was collected. Time given in hours:minutes:seconds UTC.

Figure 8. Example infragravity swash event from the ebbing portion of tide 7. A) Water depth. Cross-shore (black) and alongshore (gray) velocities from approximately 0.02 m above the bed. Time given in hours:minutes:seconds UTC. Cross-shore (C) and alongshore (D) velocity profiles. The color shading of the profiles corresponds to colored vertical lines in (B).

Figure 9. The same infragravity swash event as shown in Figure 8. A) Cross-shore (black) and alongshore (gray) velocity from 0.02 m above the bed. B) Magnitude of the cross-shore (black) and alongshore (gray) bed shear stress. C) Friction coefficient associated with cross-shore flow. Time given in hours:minutes:seconds UTC.

Journal of Waterway, Port, Coastal, and Ocean Engineering. Submitted November 29, 2012; accepted May 2, 2013; posted ahead of print May 4, 2013. doi:10.1061/(ASCE)WW.1943-5460.0000210

Figure 10. Hydrodynamics from tide 7. A) Water depth from the upper buried pressure transducer. B) Magnitude of the cross-shore (black) and alongshore (gray) bed shear stress. C) Friction coefficient associated with cross-shore flow. Time given in hours:minutes:seconds UTC. Note that the data gap following ~16:45 is due to data collection error and the sparse data following 18:15 often due to shallow water depths affecting sensor performance.

Figure 11. Histogram of friction coefficient for onshore-directed (solid) and offshore-directed (dotted) flows.

Figure 12. Velocity and sediment concentration during the ebbing portion of tide 7. A) Water depth from the upper buried pressure transducer (black), UDM (dark gray), LiDAR (dashed light gray). B) Cross-shore velocity from the lower EMCM (black) and from a bin at roughly 0.03 m above the bed from the PC-ADCP (gray). Positive velocities are onshore-directed. Gaps in the time series are when the water level was below the height of the current meter or due to other quality control procedures. C) SSC from the 5 activated FOBS sensors. Time series are offset vertically by 400 kg m-3. Bold portions of the curve indicate the bed level. D) SFSC from the CCP for various channels with channel number increments corresponding to 0.001 m. Time series are offset vertically by 1800 kg m-3. Black dots on the curves indicate the bed level. Channels below the vertical location of the dots are located within the bed. Time given in hours:minutes:seconds UTC.

Journal of Waterway, Port, Coastal, and Ocean Engineering. Submitted November 29, 2012; accepted May 2, 2013; posted ahead of print May 4, 2013. doi:10.1061/(ASCE)WW.1943-5460.0000210

Figure 13. Sediment mobilization and transport during the ebbing portion of tide 7. A) Example time series of water depth. B) Suspended load (gray) and sheet load (black). C) Suspended load transport (gray) and sheet load transport (black). Time given in hours:minutes:seconds UTC.

Figure 1

Journal of Waterway, Port, Coastal, and Ocean Engineering. Submitted November 29, 2012; accepted May 2, 2013;
posted ahead of print May 4, 2013. doi:10.1061/(ASCE)WW.1943-5460.0000210

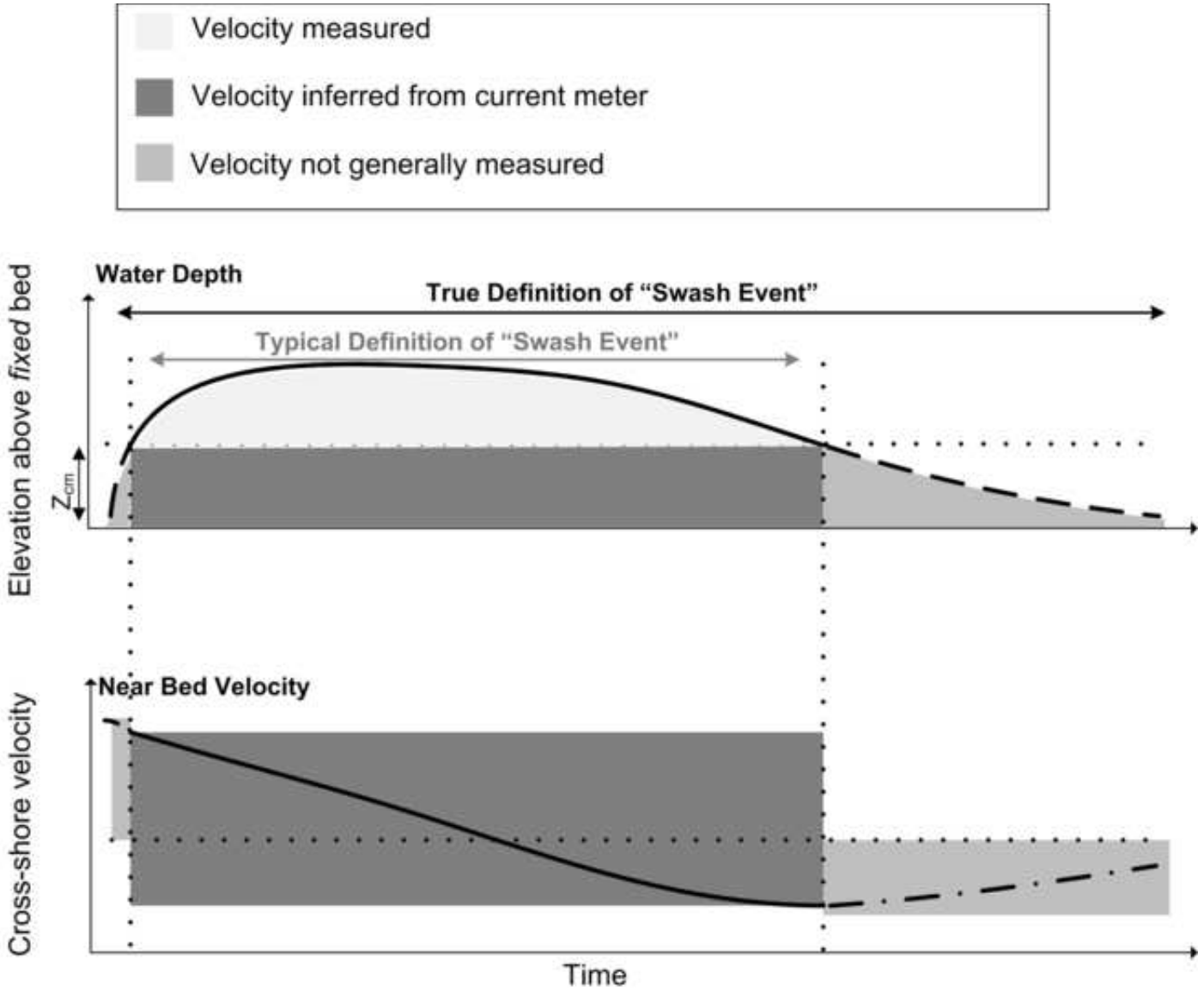

Figure 2

Journal of Waterway, Port, Coastal, and Ocean Engineering. Submitted November 29, 2012; accepted May 2, 2013; posted ahead of print May 4, 2013. doi:10.1061/(ASCE)WW.1943-5460.0000210

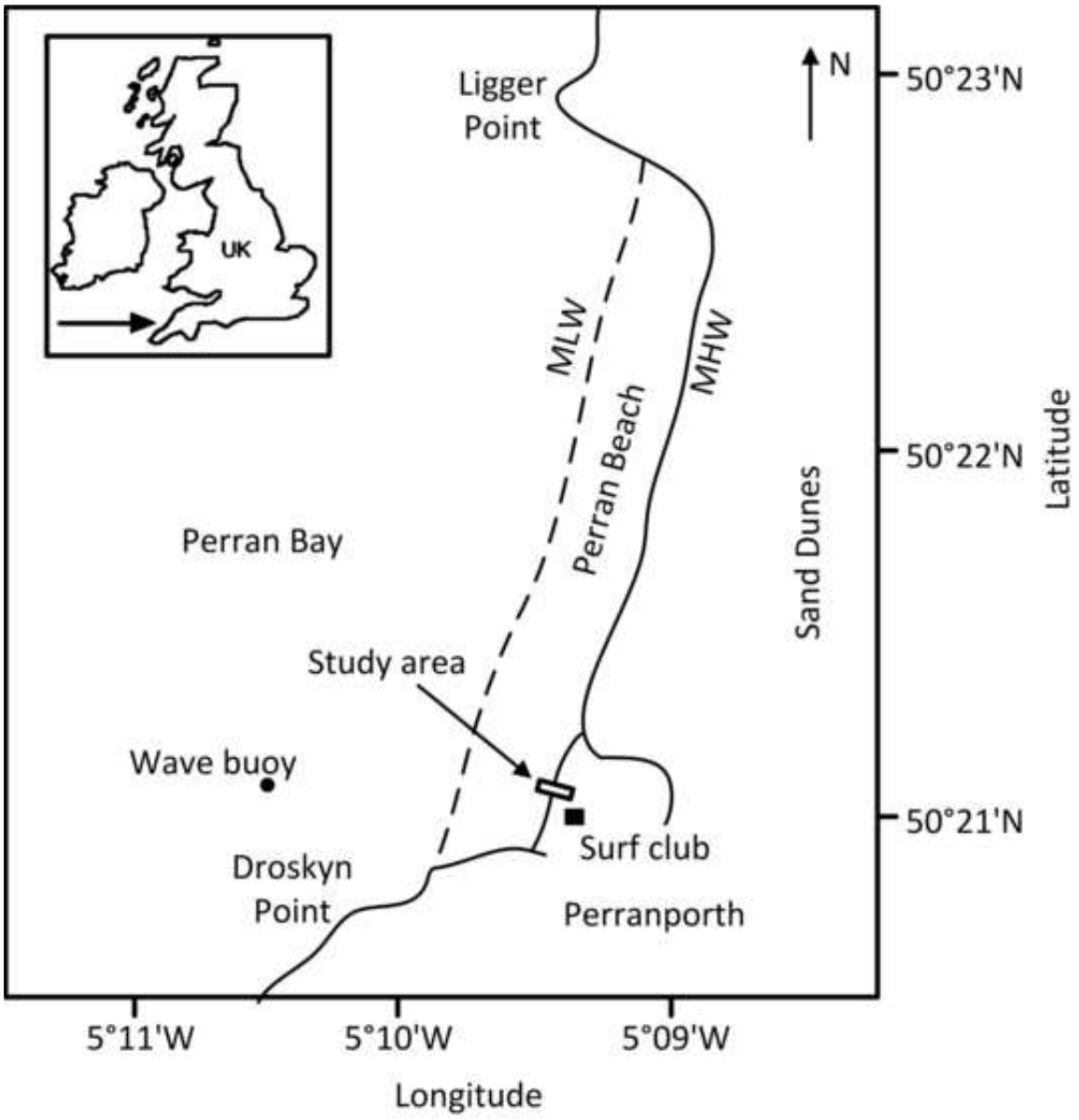

Figure 3

Journal of Waterway, Port, Coastal, and Ocean Engineering. Submitted November 29, 2012; accepted May 2, 2013;
posted ahead of print May 4, 2013. doi:10.1061/(ASCE)WW.1943-5460.0000210

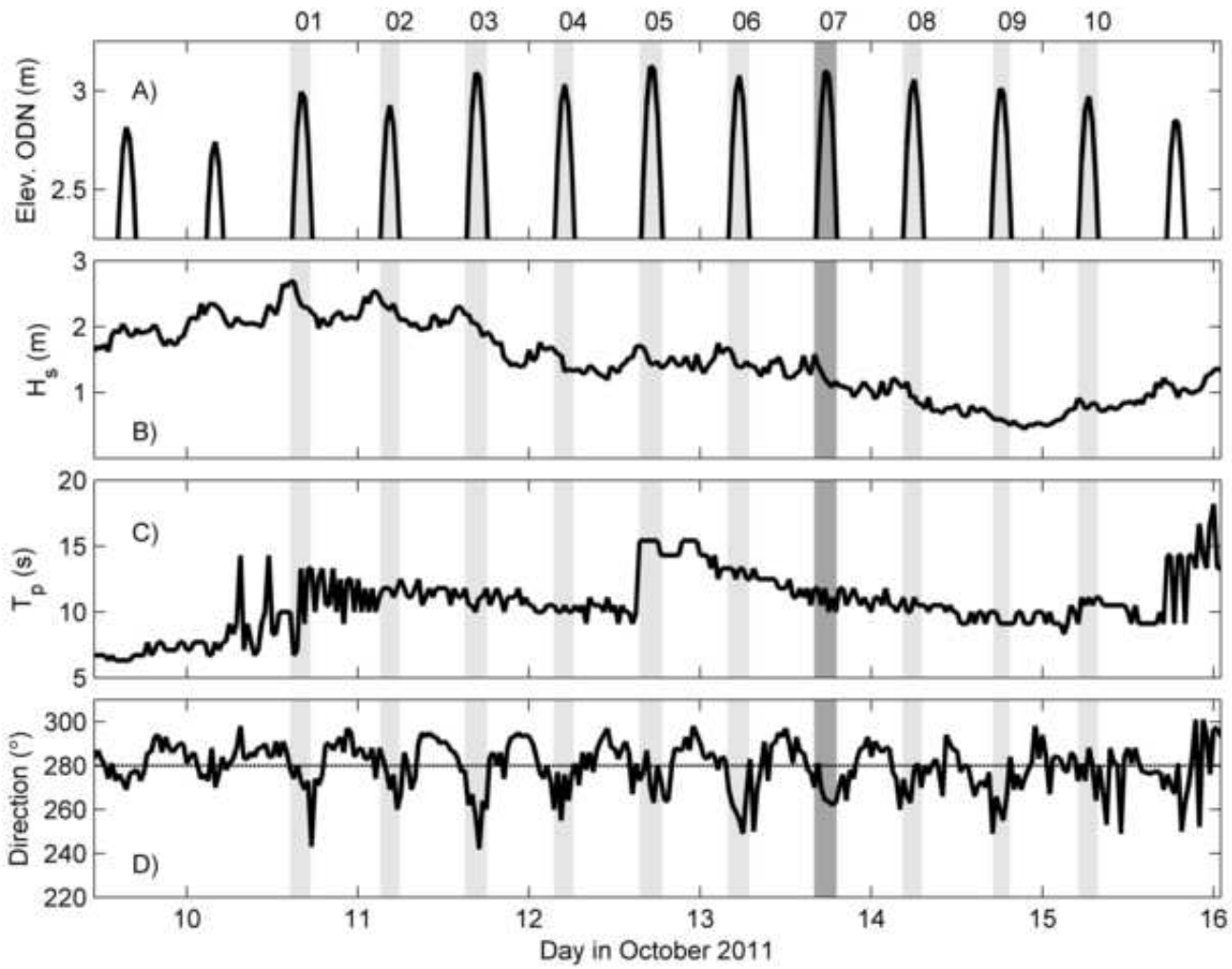

Figure 4

Journal of Waterway, Port, Coastal, and Ocean Engineering. Submitted November 29, 2012; accepted May 2, 2013;
posted ahead of print May 4, 2013. doi:10.1061/(ASCE)WW.1943-5460.0000210

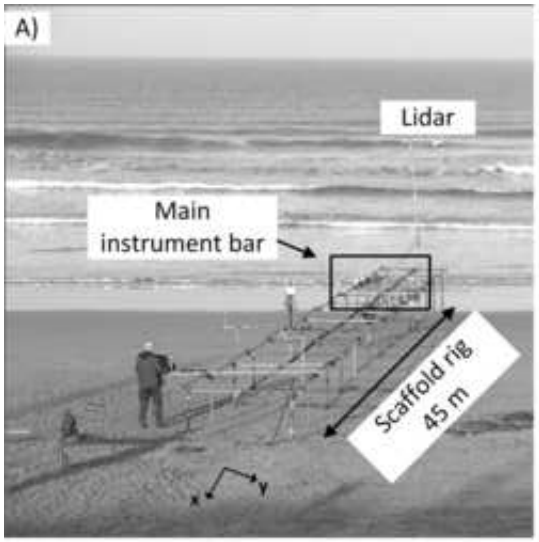

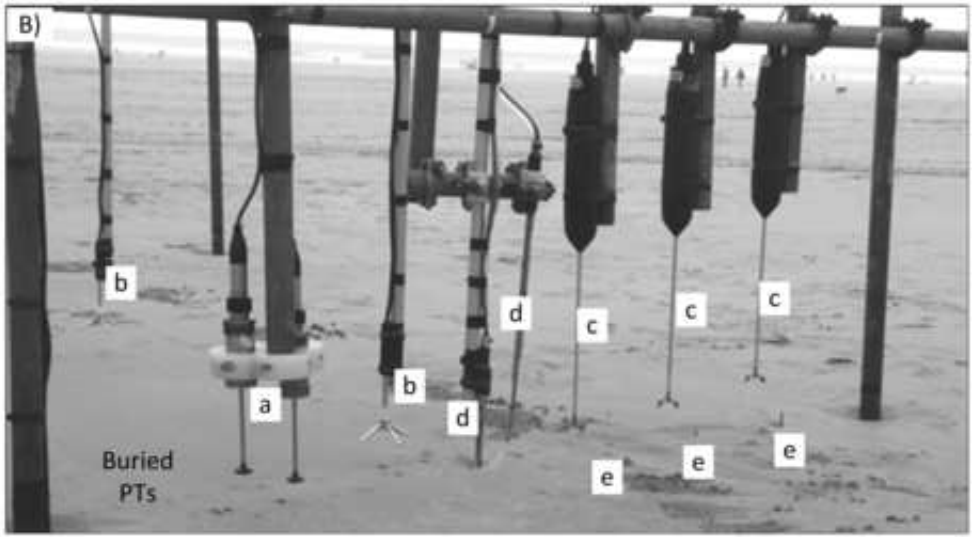

Figure 5

Journal of Waterway, Port, Coastal, and Ocean Engineering. Submitted November 29, 2012; accepted May 2, 2013;
posted ahead of print May 4, 2013. doi:10.1061/(ASCE)WW.1943-5460.0000210

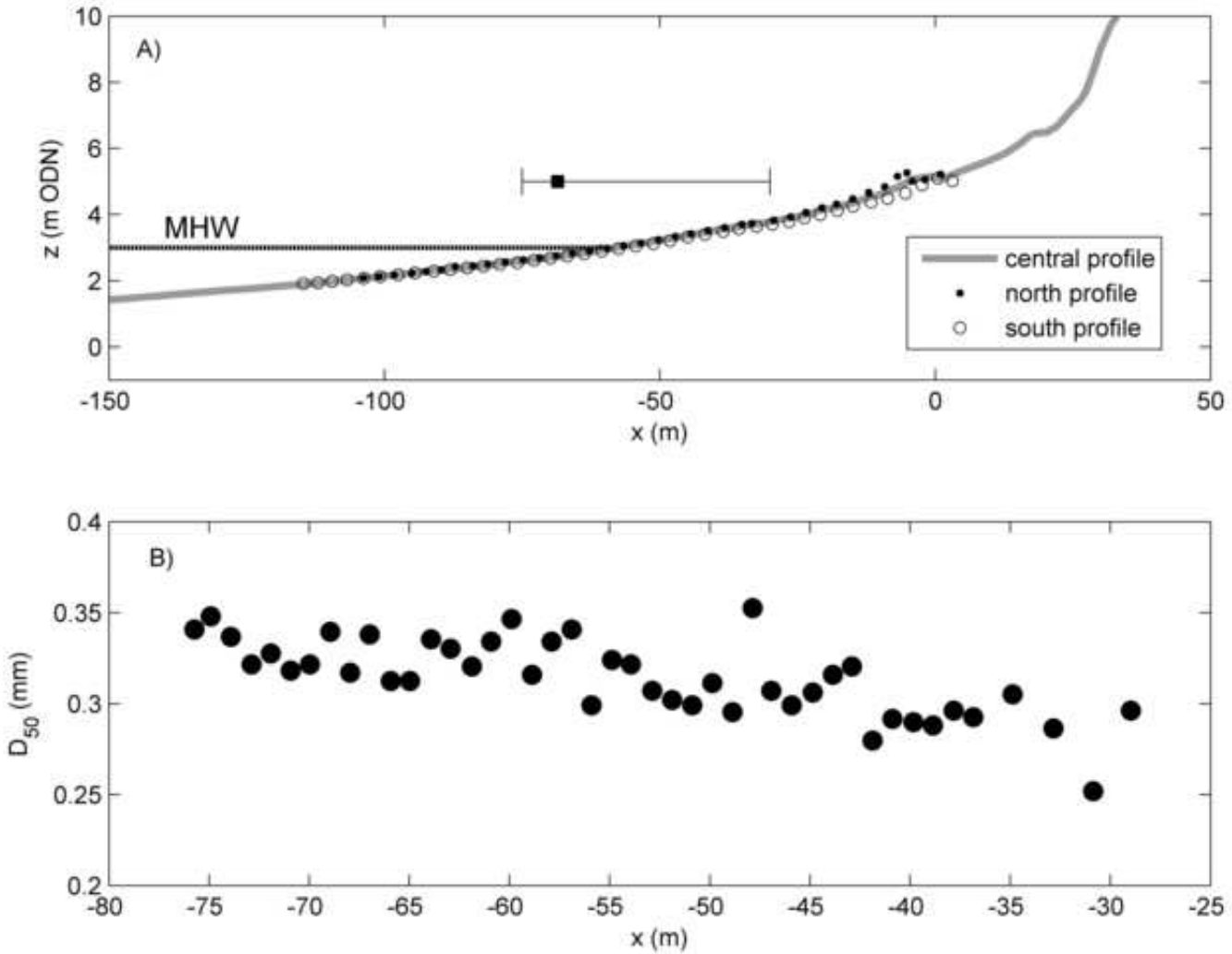

Figure 6

Journal of Waterway, Port, Coastal, and Ocean Engineering. Submitted November 29, 2012; accepted May 2, 2013;
posted ahead of print May 4, 2013. doi:10.1061/(ASCE)WW.1943-5460.0000210

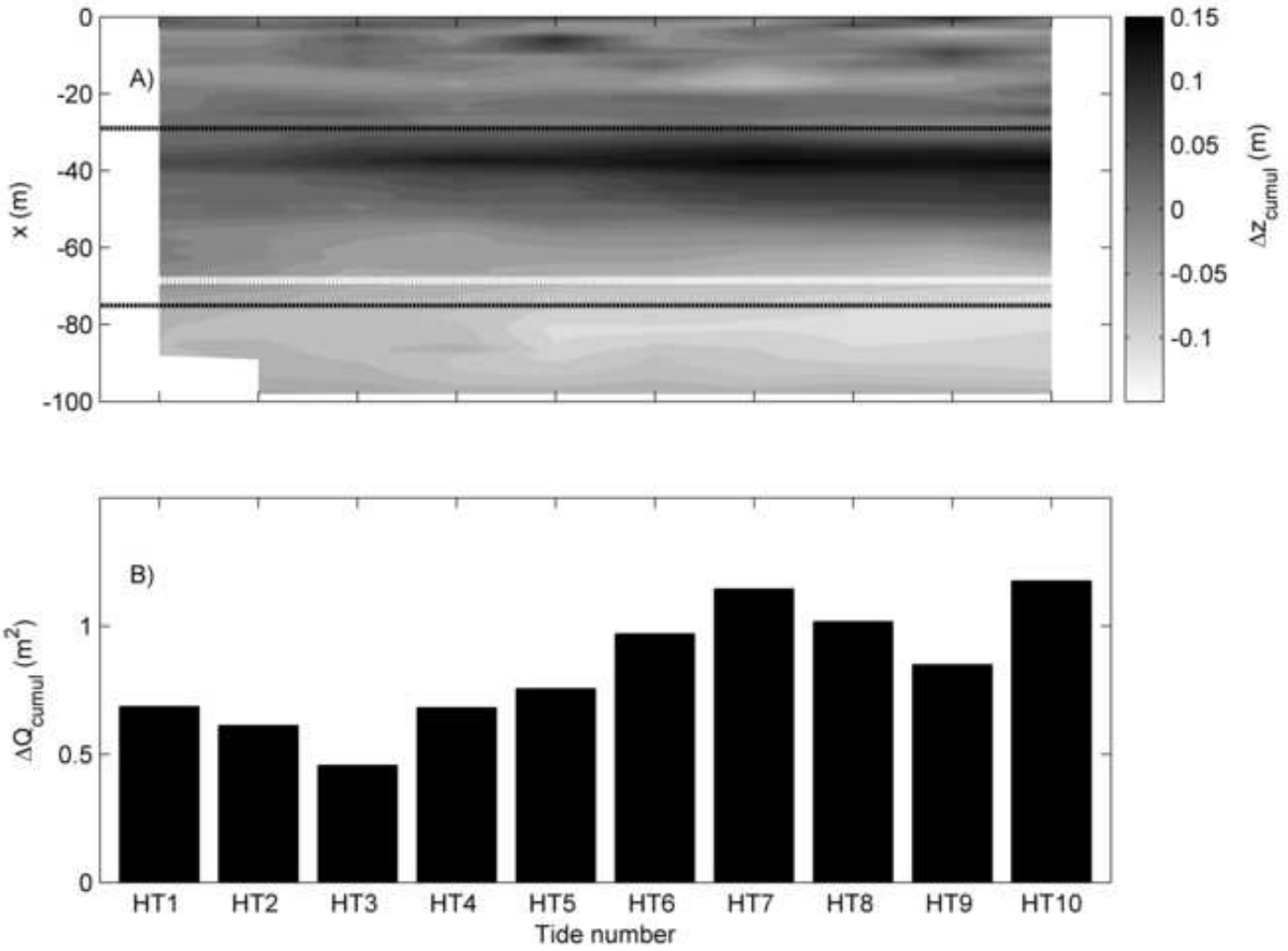

Figure 7 color

Journal of Waterway, Port, Coastal, and Ocean Engineering. Submitted November 29, 2012; accepted May 2, 2013;
posted ahead of print May 4, 2013. doi:10.1061/(ASCE)WW.1943-5460.0000210

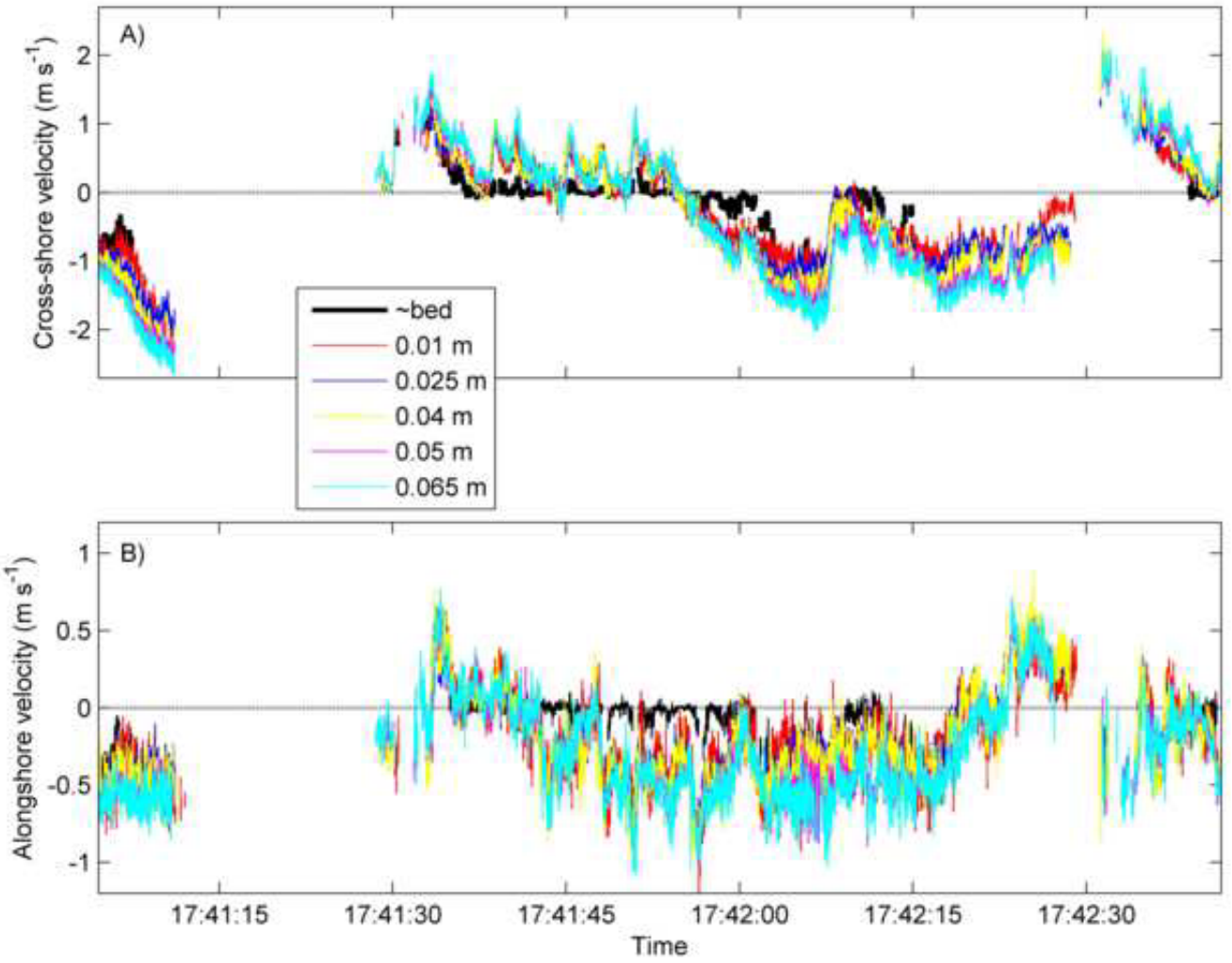

Figure 7 gray

Journal of Waterway, Port, Coastal, and Ocean Engineering. Submitted November 29, 2012; accepted May 2, 2013;
posted ahead of print May 4, 2013. doi:10.1061/(ASCE)WW.1943-5460.0000210

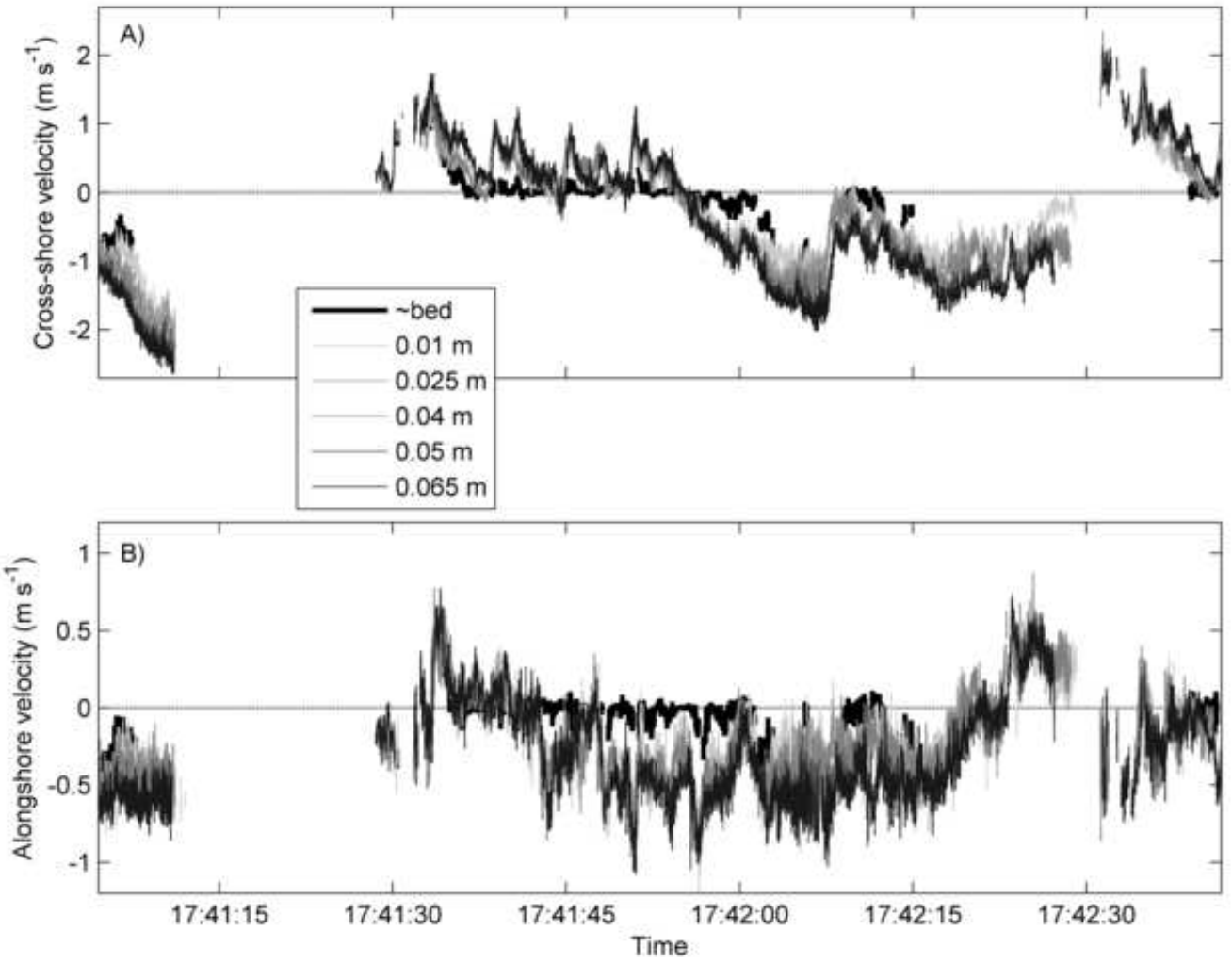

Figure 8 color

Journal of Waterway, Port, Coastal, and Ocean Engineering. Submitted November 29, 2012; accepted May 2, 2013;
posted ahead of print May 4, 2013. doi:10.1061/(ASCE)WW.1943-5460.0000210

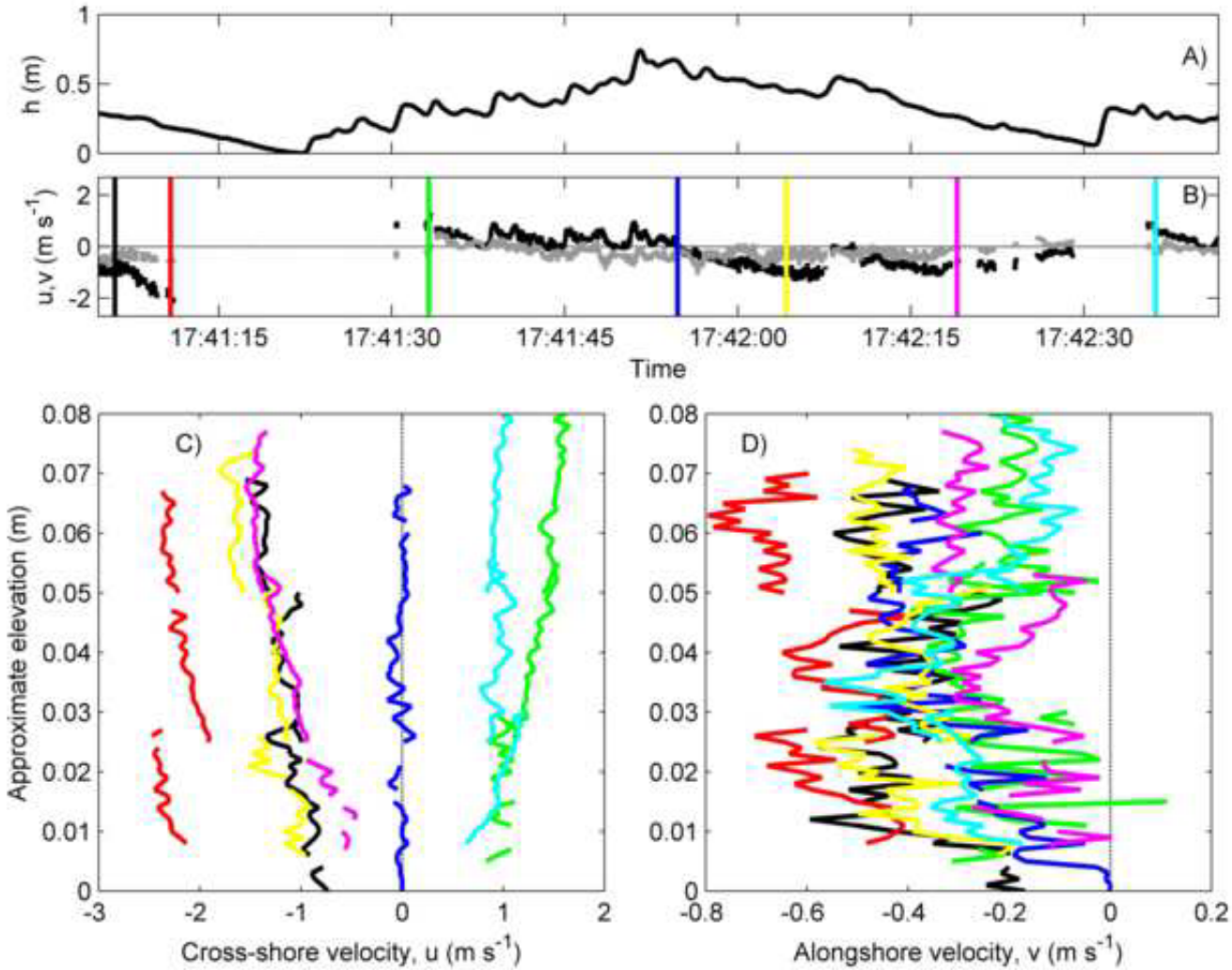

Figure 8 gray

Journal of Waterway, Port, Coastal, and Ocean Engineering. Submitted November 29, 2012; accepted May 2, 2013;
posted ahead of print May 4, 2013. doi:10.1061/(ASCE)WW.1943-5460.0000210

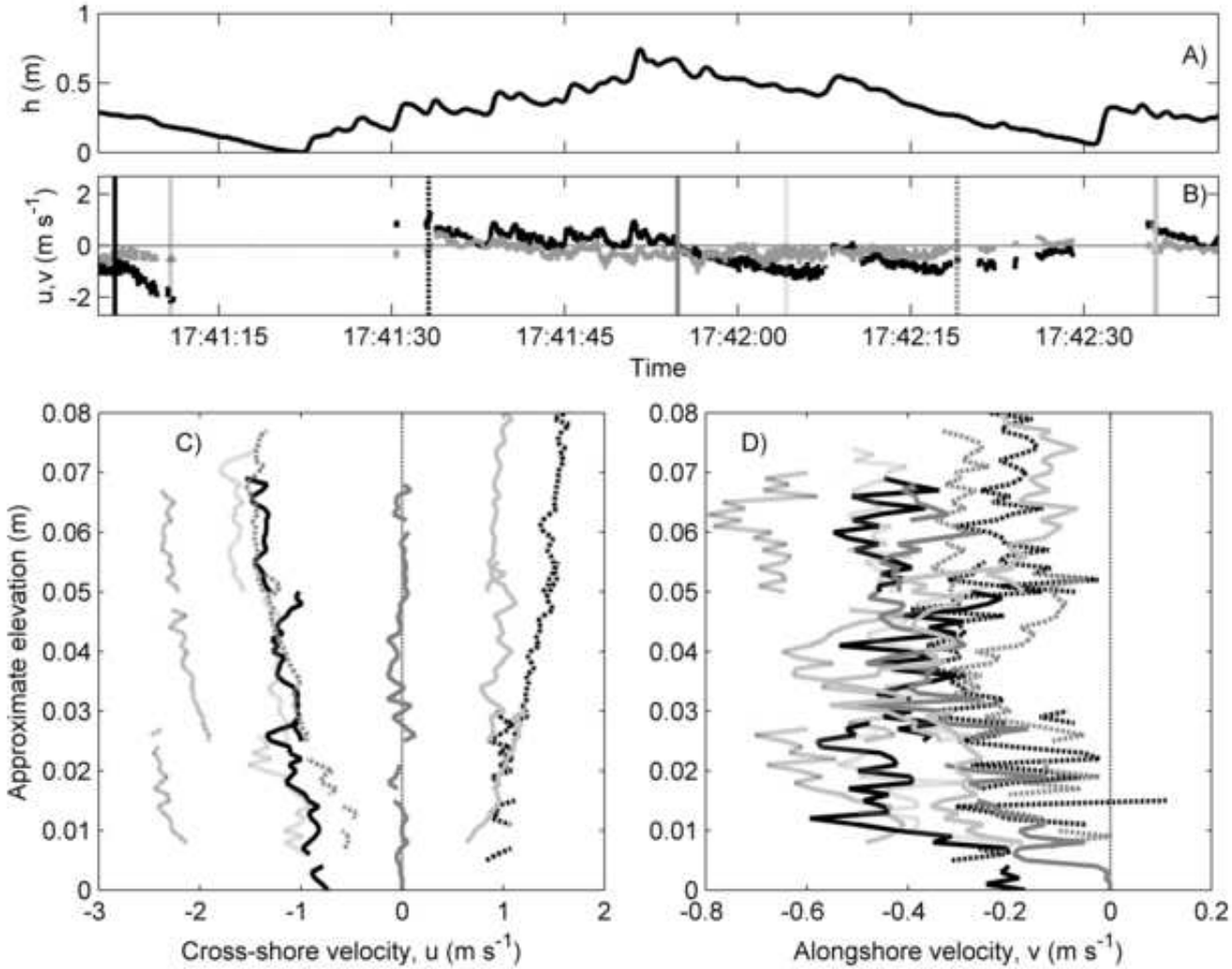

Figure 9

Journal of Waterway, Port, Coastal, and Ocean Engineering. Submitted November 29, 2012; accepted May 2, 2013;
posted ahead of print May 4, 2013. doi:10.1061/(ASCE)WW.1943-5460.0000210

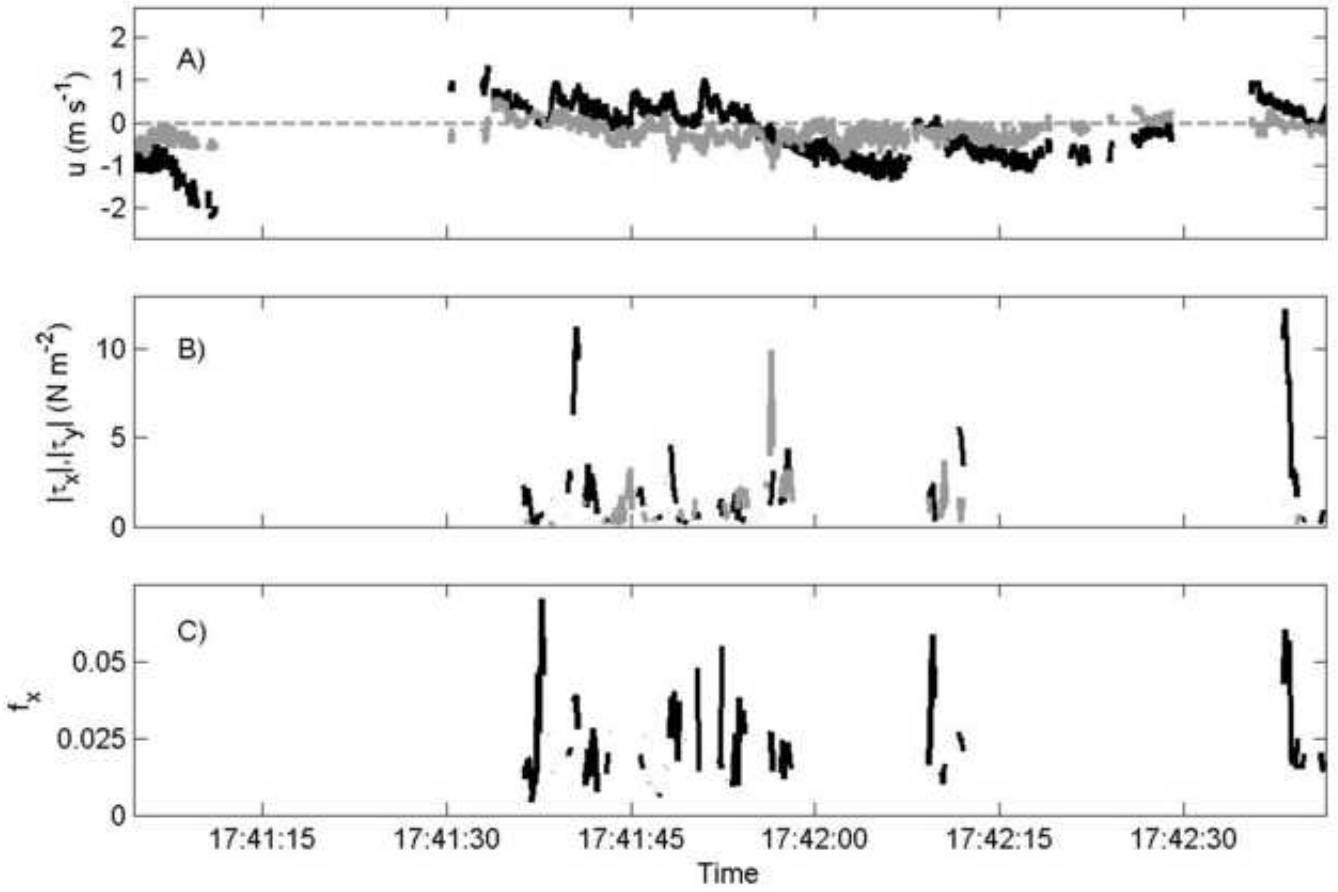

Journal of Waterway, Port, Coastal, and Ocean Engineering. Submitted November 29, 2012; accepted May 2, 2013;
posted ahead of print May 4, 2013. doi:10.1061/(ASCE)WW.1943-5460.0000210

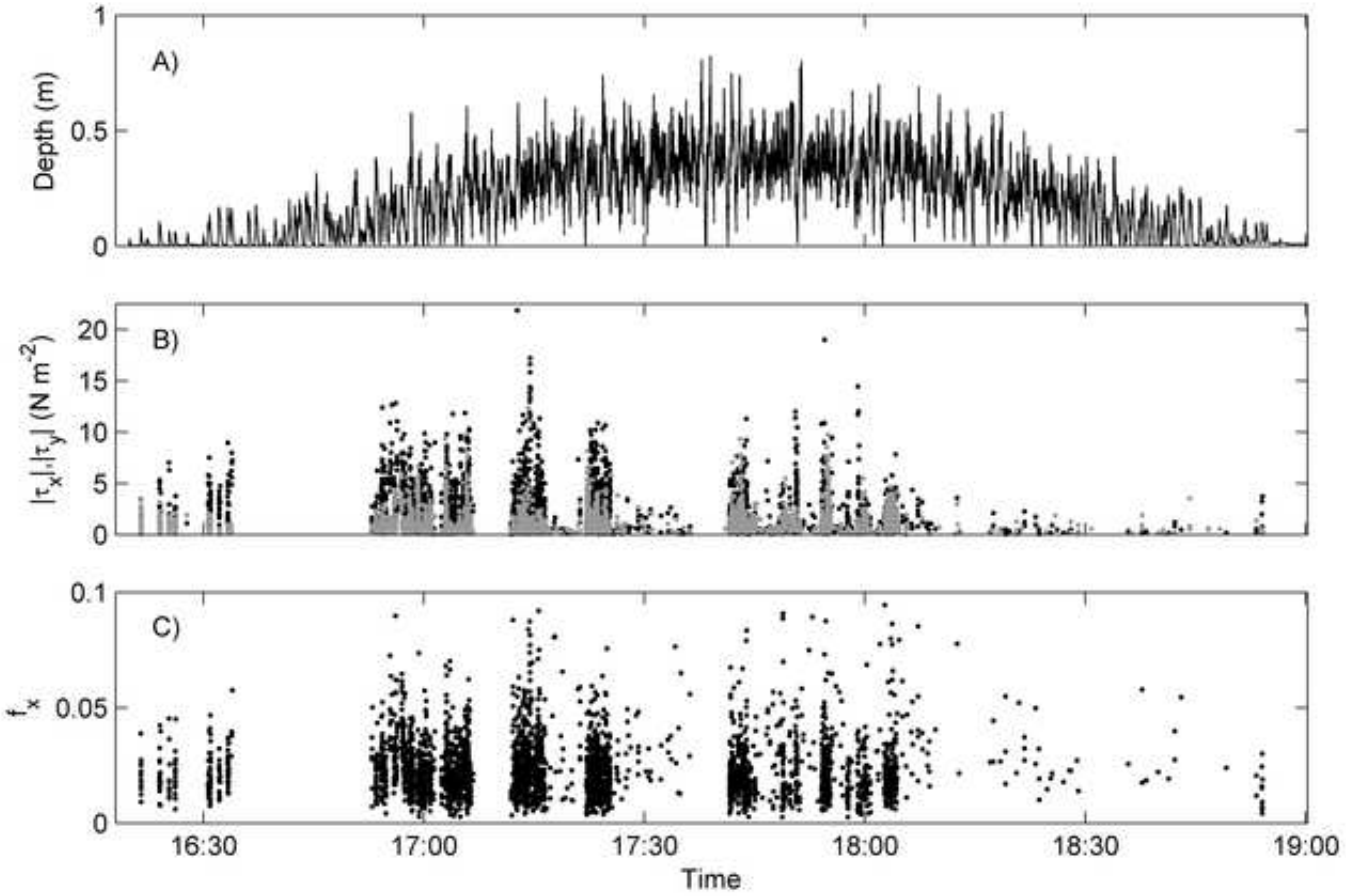

Journal of Waterway, Port, Coastal, and Ocean Engineering. Submitted November 29, 2012; accepted May 2, 2013;
posted ahead of print May 4, 2013. doi:10.1061/(ASCE)WW.1943-5460.0000210

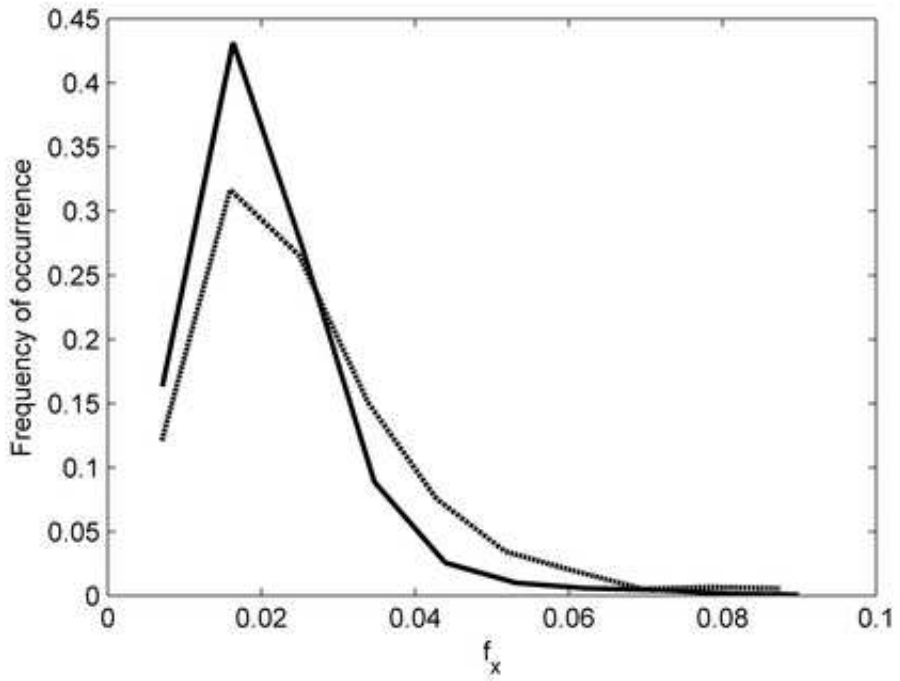

Journal of Waterway, Port, Coastal, and Ocean Engineering. Submitted November 29, 2012; accepted May 2, 2013;
posted ahead of print May 4, 2013. doi:10.1061/(ASCE)WW.1943-5460.0000210

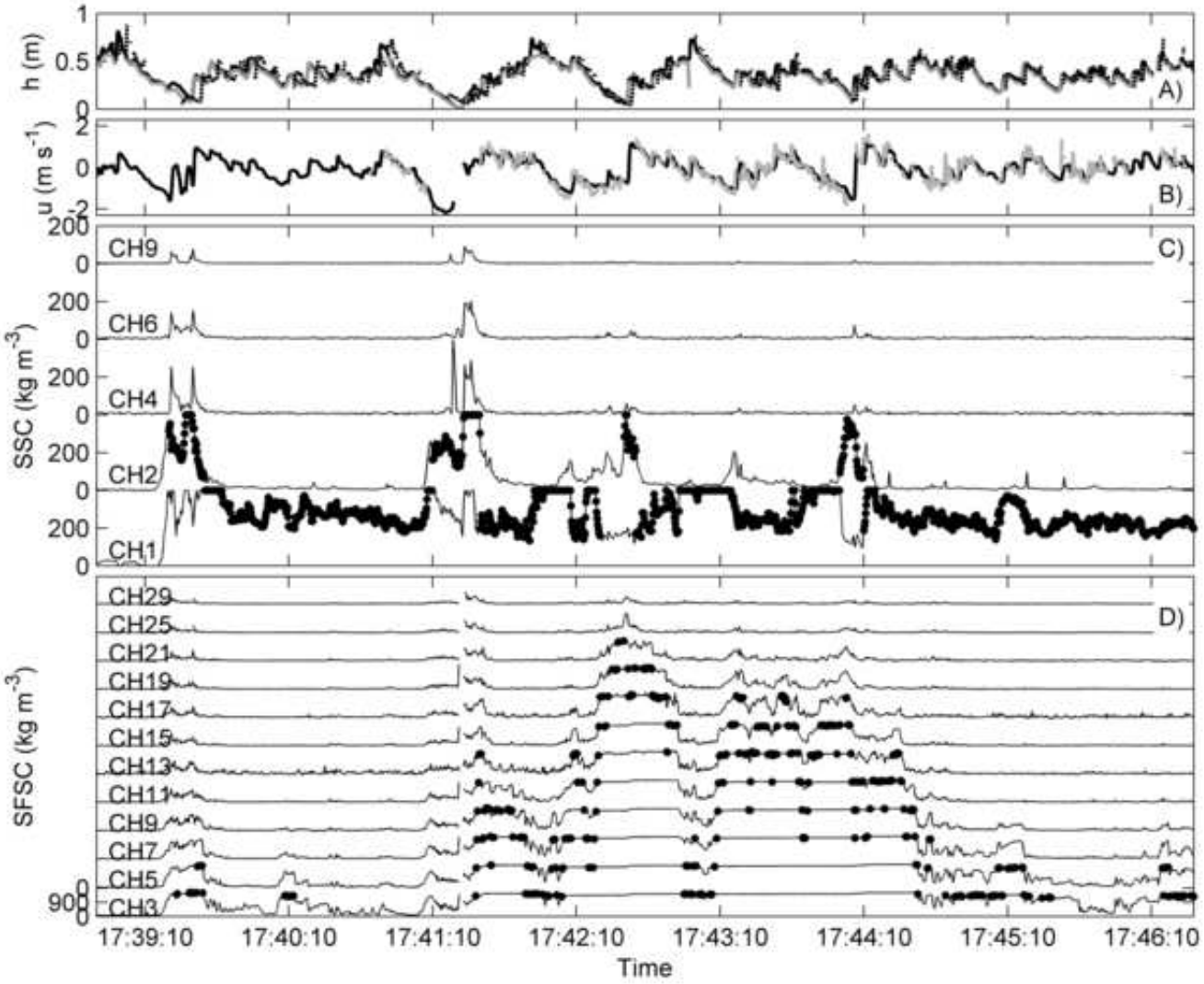

Journal of Waterway, Port, Coastal, and Ocean Engineering. Submitted November 29, 2012; accepted May 2, 2013;
posted ahead of print May 4, 2013. doi:10.1061/(ASCE)WW.1943-5460.0000210